Electronic Supplementary Material (ESI) for Chemical Science.

Electronic Supplementary Information

Core extension of alkylene-encapsulated perylene bisimides

Shunfeng Peng,[a] Zhiye Zheng,[a] Shijie Chen,[a] Hui Zhang[b] and Hongyu Wang*[a]

[a] Department of Chemistry, College of Science, and Center for Supramolecular Chemistry & Catalysis, Shanghai University, 99 Shangda Road, Shanghai, 200444, P. R. China. E-mail: wanghy@shu.edu.cn

[b] Laboratory for Microstructures, Instrumental Analysis and Research Center, Shanghai University, Shanghai 200444, P. R. China

† These authors contributed equally to this work.

Table of contents

1. General Experimental

1,6,7,12-Tetrachloroperylene-3,4,9,10-tetracarboxylic dianhydride was from Bide Pharmatech (Shanghai, China). Diethylsilane, 2,6-diisopropylaniline, 2,6-dimethoxyaniline, [1,1'-bis(di-tert-butylphosphino)ferrocene]palladium(II) dichloride, tetrabutylammonium fluoride, tetrabutylammonium chloride, tetrabutylammonium bromide, tetrabutylammonium iodide, tetrabutylammonium acetate, tetrabutylammonium hydrogen sulfate, tetrabutylammonium nitrate, and tetrabutylammonium perchlorate were purchased from Titan Scientific (Shanghai, China). Unless otherwise stated, all reagents and solvents were used as received. All reactions were performed under a nitrogen atmosphere and in dry solvents, unless otherwise stated. Flash column chromatography was performed over silica gel (200-300 mesh or 300-400 mesh).

^{1}H NMR and ^{13}C NMR spectra were recorded on a JNM-ECZ400S/L 400 MHz NMR spectrometer or a Bruker Advance 600 MHz spectrometer at ambient temperature using tetramethylsilane (TMS) as the internal standard. The chemical shifts are listed in ppm on the δ scale and coupling constants were recorded in Hz. ^{1}H NMR and ^{13}C NMR chemical shifts are reported in units of δ, parts per million (ppm), relative to the chemical shift of the residual solvent. Multiplicities were given as: s (singlet), d (doublet), t (triplet), q (quartet), m (multiplet), and br (broad). The number of protons (n) for a given resonance is indicated by nH. Coupling constants are reported as J values in Hz. Chemical shifts are calibrated relative to the signals of the non-deuterated solvents ($CDCl_3$: δ 7.26 ppm, DMSO-d_6: δ 2.50 ppm). Molecular masses were determined by Bruker ultraflextreme matrix assisted laser desorption/ionization time-of-flight mass spectrometry (MALDI-TOF MS).

UV-Vis spectra were recorded on a Saier 3600iPlus spectrophotometer. Fluorescence measurements were carried out using a Shimadzu RF6000 spectrofluorophotometer using a Xenon lamp as the light source. All the UV-Vis absorption and fluorescence measurements were performed in a standard 1 cm quartz cell at room temperature.

For femtosecond transient absorption spectroscopy, the fundamental output from Yb:KGW laser (1030 nm, 220 fs Gaussian fit, 100 kHz, Light Conversion Ltd) was separated into two light beams. One was introduced to NOPA (ORPHEUS-N, Light Conversion Ltd) to produce a certain wavelength for pump beam (here we use 550 and 750 nm, 30 fs pulse duration), the other was focused onto a YAG plate to generate white light continuum as the probe beam. The

pump and probe overlapped on the sample at a small angle of less than 10°. The transmitted probe light from the sample was collected by a linear CCD array.[1]

Thermogravimetric analyses (TGA) were carried out on a DSCQ1000 gravimetric thermal analyzer.

Powder X-ray diffraction patterns were recorded on a Rigaku D/Max2500V/PC X-ray powder diffractometer with Cu-Kα radiation (λ = 0.15418 nm).

X-ray crystallographic analyses were carried out on an Agilent Technologies SuperNova Dual Source diffractometer using a μ-focus Cu Kα radiation source (λ = 1.5418 Å) or Ga Kα (λ = 1.34139 Å) with collimating mirror monochromators. Data were collected using □-scans. The structures were solved by direct methods using SHELXT and refined by full-matrix least-squares on F^2 with anisotropic displacement parameters for the non-H atoms using SHELXL-2018/3. Structure analysis was aided by use of the programs PLATON and OLEX2. X-ray crystallographic coordinates for the structures reported in this study have been deposited at the Cambridge Crystallographic Data Centre (CCDC) under deposition numbers 2464307, 2464308, 2464309, and 2464311.

Cyclic voltammetry (CV) was performed in dry dichloromethane at a scanning rate of 50 mV s^{-1} on a PC-controlled electrochemical analyzer (CH Instruments CHI 660E) under a nitrogen atmosphere. Measurements were carried out in a glass vial using a glassy carbon, an Ag/Ag^+ and a Pt wire as working, reference and counter electrodes, respectively. The electrolyte was Tetra-n-butylammonium hexafluorophosphate ($TBAPF_6$, 0.1 M) was used as the supporting electrolyte. All potentials are reported relative to the ferrocene/ferrocenium couple (Fc/Fc^+), which was used as an external standard to calibrate the reference electrode.

All calculations were carried out using the Gaussian 16 program.[2] Initial geometries were obtained from the single crystals of the encapsulated DPPs. The structures were fully optimized without any symmetry restriction. Density functional theory (DFT) computations were performed in the gas-phase geometry optimization using B3LYP-D3 functional and the 6-311G(d,p) basis set. The time-dependent DFT (TD-DFT) method at the B3LYP/6311G(d,p) level was employed to simulate the vertical excitations of these compounds. The results were visualized using GaussView software and Multiwfn 3.8 program.[3,4]

2. Synthesis

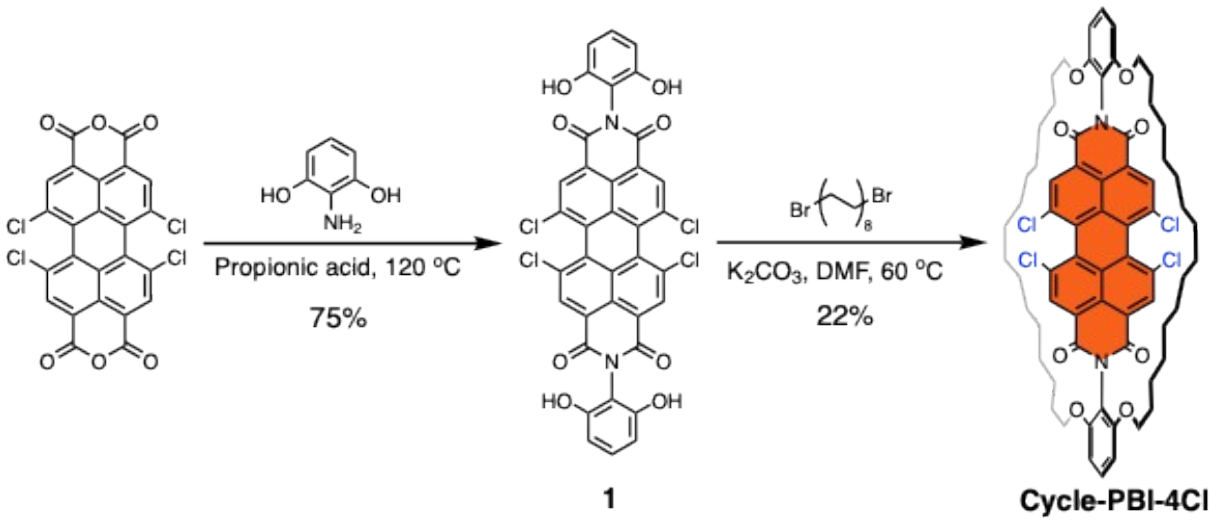

Scheme S1. Synthesis of tetrachloro-substituted **Cycle-PBI-4Cl**.

Compound 1

1,6,7,12-Tetrachloroperylene-3,4,9,10-tetracarboxylic dianhydride (2.6 g, 5 mmol) and 2,6-dihydroxyaniline (2.7 g, 21.5 mmol) were added to a 250 mL round-bottom flask, followed by the addition of propionic acid (100 mL). The mixture was heated to reflux for 24 h. After cooling to room temperature, 100 mL of water was added, and the resulting solid was filtered and washed three times with dichloromethane. The crude product was purified by silica gel column chromatography using methanol/dichloromethane (1:16, v/v) as the eluent to afford a dark red solid (1.8 g, 75% yield).

^{1}H NMR (400 MHz, DMSO-d_6) δ 9.52 (s, 4H), 8.63 (s, 3H), 7.11 (t, J = 8.2 Hz, 2H), 6.42 (d, J = 8.2 Hz, 4H). Insufficient solubility for ^{13}C NMR.

MS (MALDI-TOF): *m/z* calcd for $C_{36}H_{15}Cl_4N_2O_8$ $[M+H]^+$: 742.9583, found: 742.9586.

Cycle-PBI-4Cl

Compound **1** (900 mg, 1.2 mmol), 1,16-dibromohexadecane (1.84 g, 4.8 mmol), and potassium carbonate (1.33 g, 9.58 mmol) were dissolved in *N*,*N*-dimethylformamide (150 mL) under an argon atmosphere. The mixture was heated to 60 °C for 2 days. After cooling to room temperature, 50 mL of 10% HCl was added, and the resulting solid was filtered and washed with methanol three times. The crude product was purified by silica gel column chromatography

using petroleum ether/CH_2Cl_2 (1:1, v/v) as the eluent to afford an orange solid (318.2 mg, 22% yield).

^{1}H NMR (400 MHz, $CDCl_3$) δ 8.74 (s, 4H), 7.39 (t, J = 8.5 Hz, 2H), 6.7 (d, J = 8.5 Hz, 4H), 4.02 (t, J = 5.4 Hz, 8H), 1.61-1.58 (m, 8H), 1.26-1.16 (m, 8H), 1.09-1.02 (m, 8H), 0.78-0.71 (m, 8H), 0.54-0.52 (br, 8H), 0.45-0.41 (br, 16H).

^{13}C NMR (100 MHz, $CDCl_3$) δ 161.5, 155.9, 135.6, 133.1, 131.8, 130.7, 128.8, 123.8, 123.7, 112.4, 105.5, 69.3, 29.0, 28.9, 28.7, 28.4, 26.0.

MS (MALDI-TOF): *m/z* calcd for $C_{68}H_{75}Cl_4N_2O_8$ $[M+H]^+$: 1187.4278, found: 1187.4887; calcd for $C_{68}H_{74}Cl_4N_2O_8Na$ $[M+Na]^+$: 1209.4097, found: 1209.4581; calcd for $C_{68}H_{74}Cl_4N_2O_8K$ $[M+K]^+$: 1225.3836, found: 1225.4548.

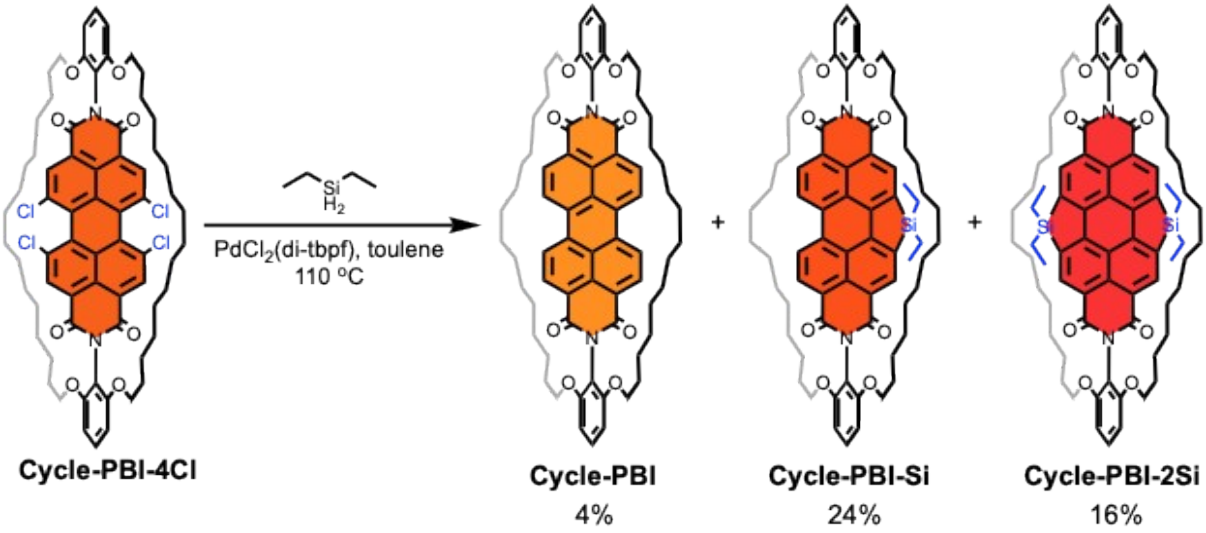

Scheme S2. Synthesis of **Cycle-PBI**, sila-annulated **Cycle-PBI-Si**, and disila-annulated **Cycle-PBI-2Si**.

Sila-annulated macrocyclic PBIs

Cycle-PBI-4Cl (300 mg, 0.25 mmol), $PdCl_2$(di-tbpf) (165 mg, 0.22 mmol), and potassium acetate (196 mg, 2 mmol) were added to a Schlenk flask under nitrogen. Diethylsilane (0.7 mL, 5 mmol) and toluene (25 mL) were added, and the mixture was refluxed for 12 h. After cooling to room temperature, the mixture was filtered and washed with CH_2Cl_2. The solvent was removed under vacuum, and the residue was purified by silica gel column chromatography using petroleum ether/CH_2Cl_2/diethyl ether (5:5:1, v/v/v) as the eluent to afford **Cycle-PBI**, monosila-annulated **Cycle-PBI-Si** and disila-annulated **Cycle-PBI-2Si** in one pot.

Cycle-PBI-2Si: Red solid (50 mg, yield: 16%).

^{1}H NMR (400 MHz, $CDCl_3$) δ 8.85 (s, 4H), 7.37 (t, J = 8.4 Hz, 2H), 6.70 (d, J = 8.6 Hz, 4H), 4.01 (t, J = 5.3 Hz, 8H), 1.59-1.53 (m, 8H), 1.28-1.21 (m, 12H), 1.19-1.11 (m, 16H), 1.08-1.0 (m, 8H), 0.8-0.72 (m, 8H), 0.53-0.46 (br, 8H), 0.41-0.37 (br, 16H).

^{13}C NMR (100 MHz, $CDCl_3$) δ 163.7, 156.0, 147.7, 137.0, 136.0, 131.0, 130.1, 122.5, 122.4, 113.6, 105.3, 69.2, 28.8, 28.6, 28.5, 28.2, 28.0, 25.8, 7.9, 3.1.

^{29}Si NMR (119 MHz, $CDCl_3$) δ 15.43.

MS (MALDI-TOF): *m/z* calcd for $C_{76}H_{95}N_2O_8Si_2$ $[M+H]^+$: 1219.6627, found: 1219.6420; calcd for $C_{76}H_{94}N_2O_8Si_2Na$ $[M+Na]^+$: 1241.6446, found: 1241.6443; calcd for $C_{76}H_{94}N_2O_8Si_2K$ $[M+K]^+$: 1257.6186, found: 1257.6239.

Cycle-PBI-Si: Orange-red solid (67 mg, yield: 24%).

^{1}H NMR (400 MHz, $CDCl_3$) δ 8.91 (s, 2H), 8.72 (d, J = 7.9 Hz, 2H), 8.58 (d, J = 8.0 Hz, 2H), 7.37 (t, J = 8.5 Hz, 2H), 6.70 (d, J = 8.5 Hz, 4H), 4.04-3.98 (m, 8H), 1.59-1.53 (m, 8H), 1.27-1.18 (m, 14H), 1.14-1.1 (m, 4H), 1.06-0.99 (m, 8H), 0.80-0.73 (br, 8H), 0.54-0.47 (br, 24H).

^{13}C NMR (100 MHz, $CDCl_3$) δ 163.7, 162.7, 156.0, 147.2, 137.1, 135.4, 132.2, 130.8, 130.2, 125.1, 123.8, 123.0, 122.6, 113.4, 105.4, 69.3, 29.0, 28.9, 28.8, 28.7, 28.5, 28.4, 26.0, 7.8, 2.8.

^{29}Si NMR (119 MHz, $CDCl_3$) δ 11.99.

MS (MALDI-TOF): *m/z* calcd for $C_{72}H_{87}N_2O_8Si$ $[M+H]^+$: 1135.6232, found: 1135.6234; calcd for $C_{72}H_{86}N_2O_8SiNa$ $[M+Na]^+$: 1157.6051, found: 1157.6062.

Cycle-PBI: Orange solid (10 mg, yield: 4%).

^{1}H NMR (600 MHz, $CDCl_3$) δ 8.77 (d, J = 7.9 Hz, 4H), 8.71 (d, J = 8.1 Hz, 4H), 7.35 (t, J = 2.5 Hz, 2H), 6.70 (d, J = 8.5 Hz, 4H), 4.01 (t, J = 5.0 Hz, 8H), 1.57-1.54 (m, 8H), 1.23-1.18 (m, 8H), 1.04-0.99 (m, 12H), 0.89-0.87 (m, 8H), 0.84-0.77 (m, 8H), 0.56-0.52 (br, 16H).

^{13}C NMR (100 MHz, $CDCl_3$) δ 162.7, 155.9, 135.0, 131.7, 130.3, 130.2, 126.9, 123.9, 123.1, 113.1 105.5, 69.3, 29.2, 29.0, 28.9, 28.8, 28.5, 26.3.

MS (MALDI-TOF): *m/z* calcd for $C_{68}H_{79}N_2O_8$ $[M+H]^+$: 1051.5836, found: 1051.5836; calcd for $C_{68}H_{78}N_2O_8Na$ $[M+Na]^+$: 1073.5656, found: 1073.5596.

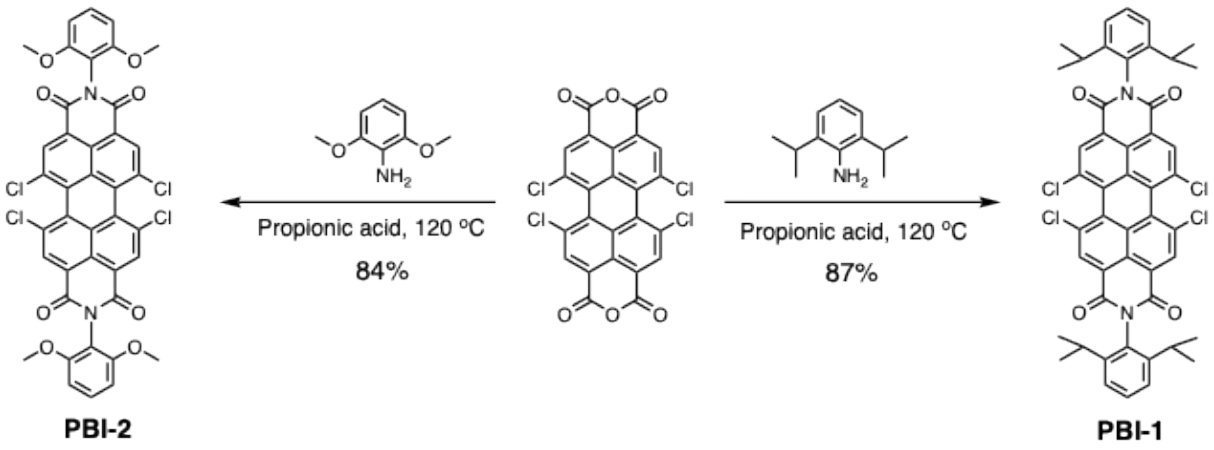

Scheme S3. Synthesis of **PBI-1** and **PBI-2**.

PBI-1

1,6,7,12-Tetrachloroperylene-3,4,9,10-tetracarboxylic dianhydride (2.6 g, 5 mmol) and 2,6-diisopropylaniline (3.5 g, 20 mmol) were added to a 250 mL round-bottom flask, followed by the addition of propionic acid (100 mL). The mixture was heated to reflux for 24 h. After cooling to room temperature, 100 mL of water was added, and the resulting solid was filtered and washed three times with methanol. The crude product was purified by silica gel column chromatography using petroleum ether/CH_2Cl_2 (1:1, v/v) as the eluent to afford an orange solid (3.7 g, 87% yield).

^{1}H NMR (400 MHz, $CDCl_3$) δ 8.77 (s, 4H), 7.52 (t, J = 7.8 Hz, 2H), 7.37 (d, J = 7.8 Hz, 4H), 2.74 (m, J = 6.9 Hz, 4H), 1.19 (dd, J = 6.9, 4.4 Hz, 24H).

^{13}C NMR (100 MHz, $CDCl_3$) δ 162.44, 145.69, 135.74, 133.56, 131.86, 130.14, 129.96, 129.03, 124.39, 124.04, 123.33, 31.68, 29.39, 24.13.

PBI-2

1,6,7,12-Tetrachloroperylene-3,4,9,10-tetracarboxylic dianhydride **1** (2.6 g, 5 mmol) and 2,6-dimethoxyaniline (3.1 g, 20 mmol) were added to a 250 mL round-bottom flask, followed by the addition of propionic acid (100 mL). The mixture was heated to reflux for 24 h. After cooling to room temperature, 100 mL of water was added, and the resulting solid was filtered and washed three times with methanol. The crude product was purified by silica gel column chromatography using dichloromethane as the eluent to afford a red solid (3.4 g, 84% yield).

^{1}H NMR (400 MHz, $CDCl_3$) δ 8.71 (s, 4H), 7.43 (t, J = 8.6 Hz, 2H), 6.73 (d, J = 8.5 Hz, 4H), 3.78 (s, 12H).

^{13}C NMR (100 MHz, $CDCl_3$) δ 161.70, 156.24, 135.41, 133.23, 131.87, 130.83, 128.80, 124.13, 123.87, 111.87, 104.53, 56.16.

3. ^{1}H NMR、^{13}C NMR Spectra and Mass Spectra

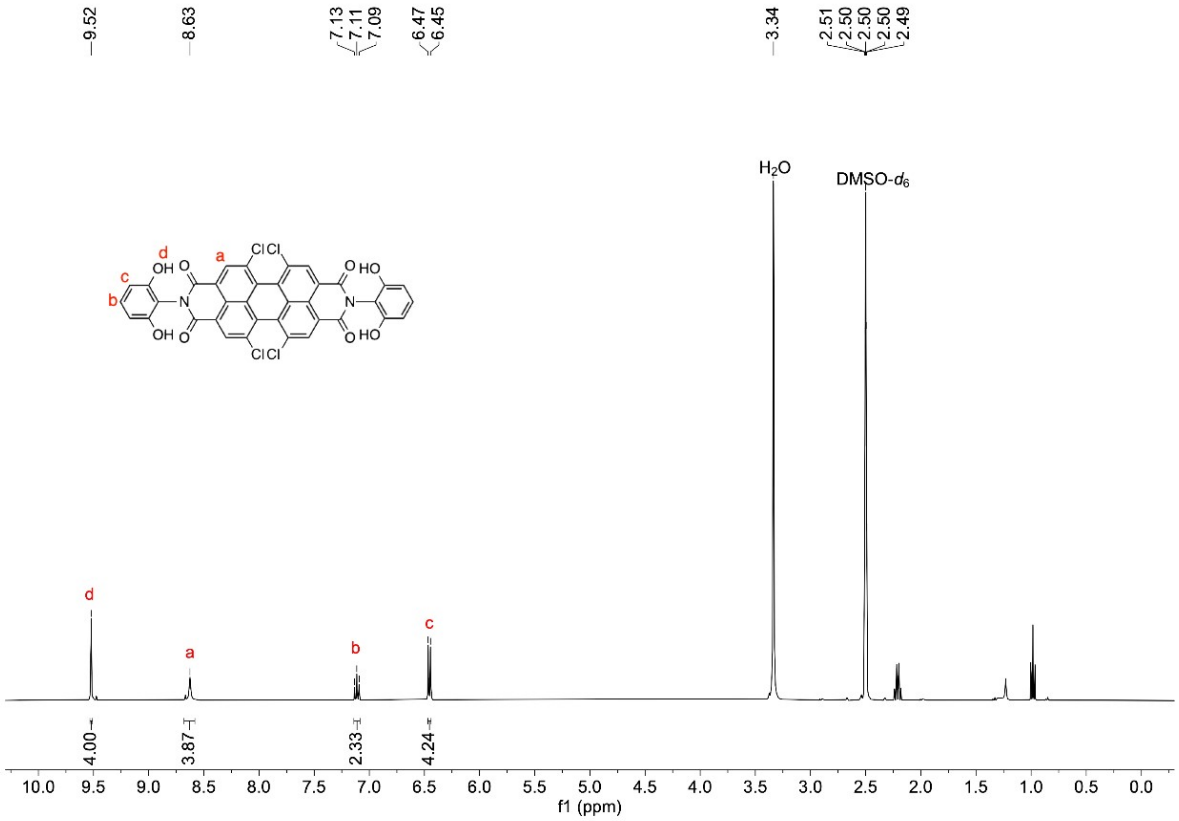

Figure S1. ^{1}H NMR spectrum of compound **1** in DMSO-d_6.

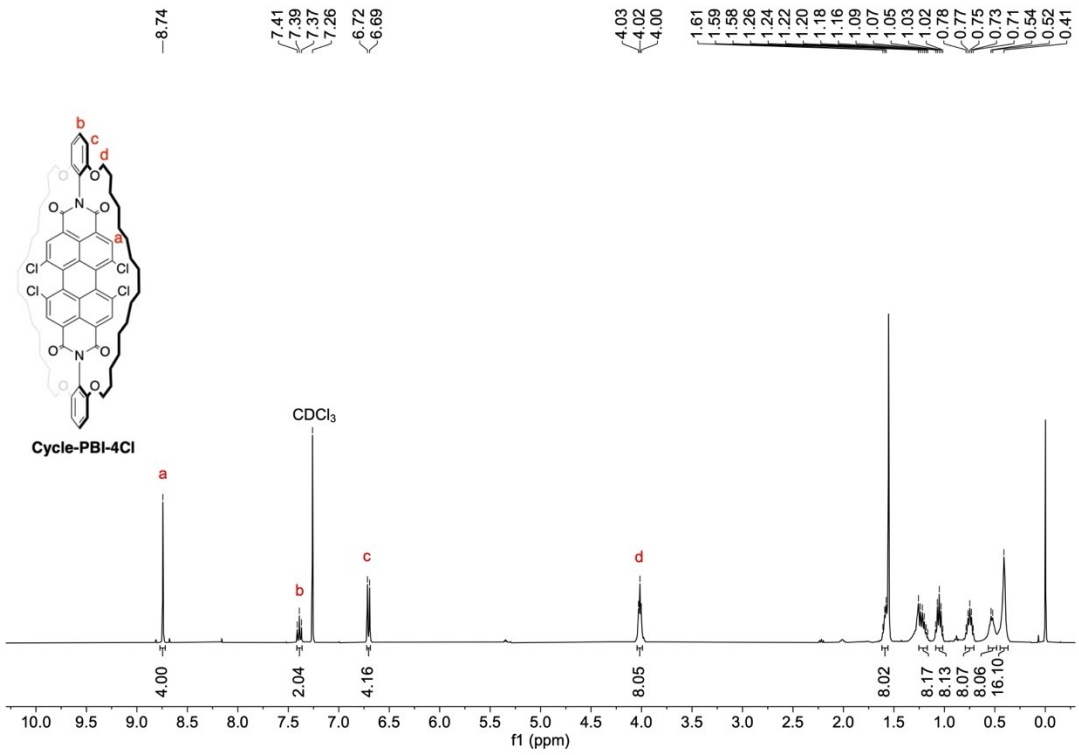

Figure S2. ^{1}H NMR spectrum of **Cycle-PBI-4Cl** in $CDCl_3$.

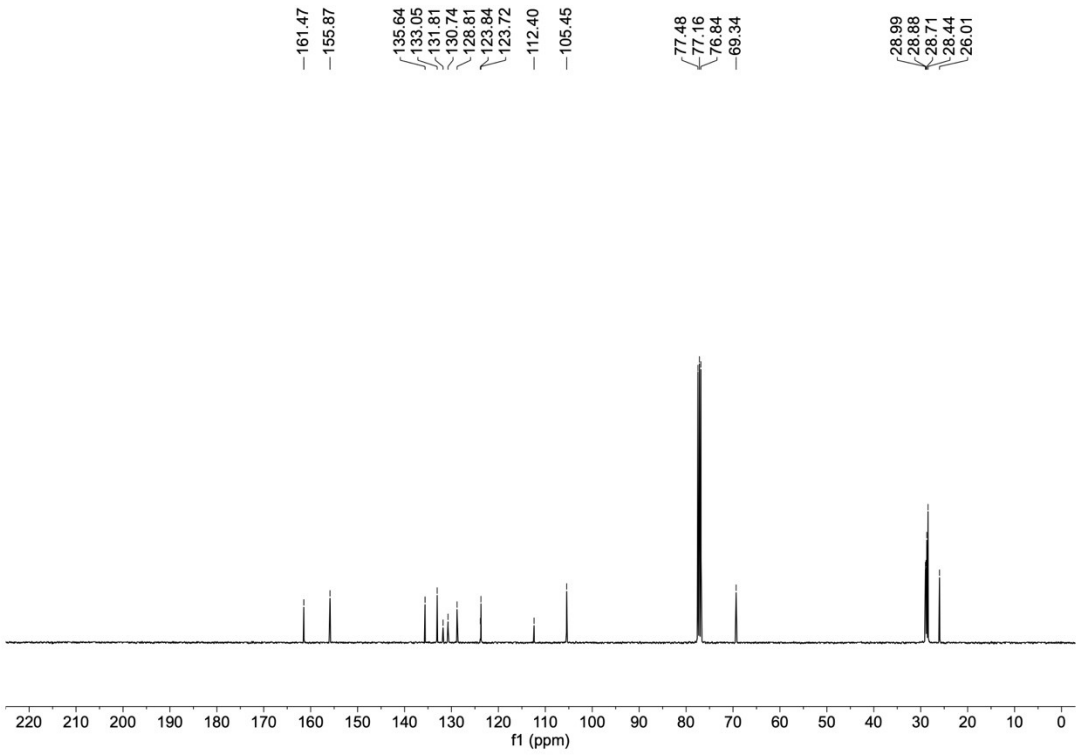

Figure S3. ^{13}C NMR spectrum of **Cycle-PBI-4Cl** in $CDCl_3$.

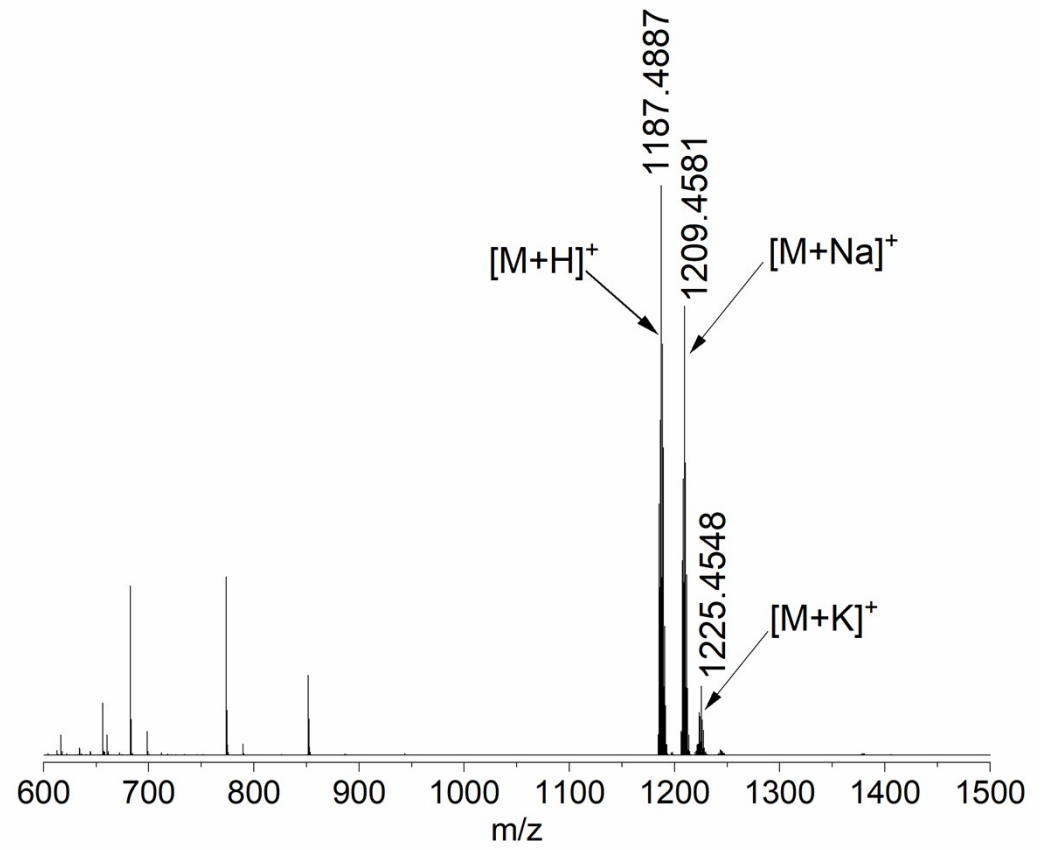

Figure S4. MALDI-TOF mass spectrum of **Cycle-PBI-4Cl**.

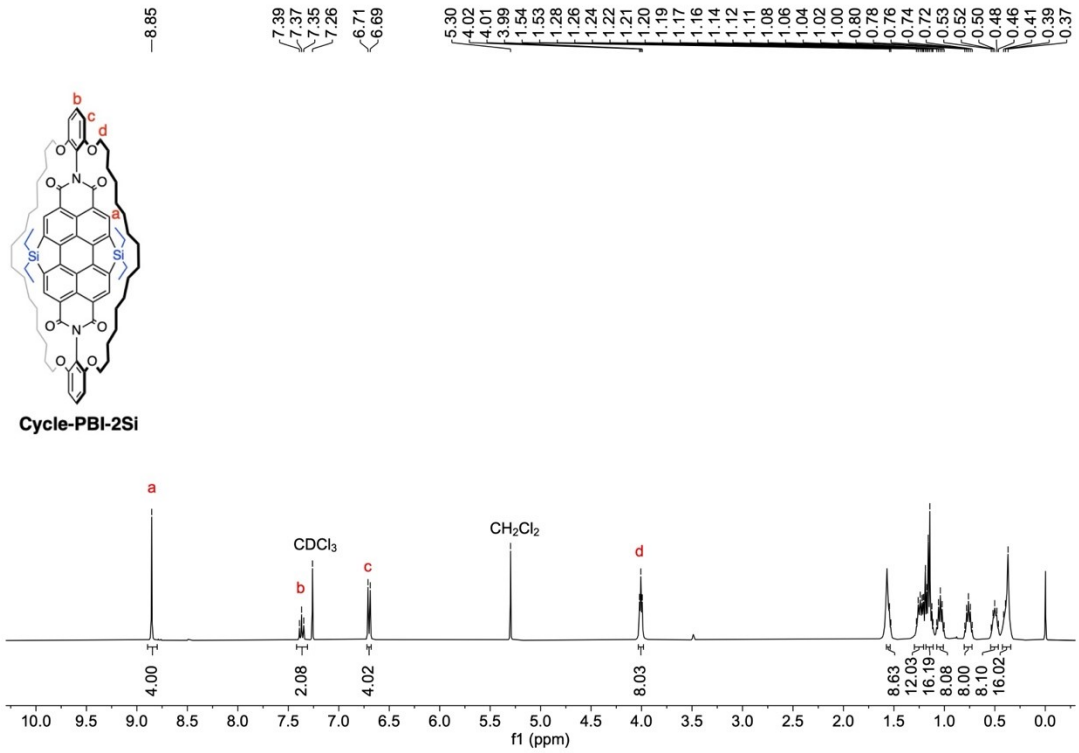

Figure S5. ^{1}H NMR spectrum of **Cycle-PBI-2Si** in $CDCl_3$.

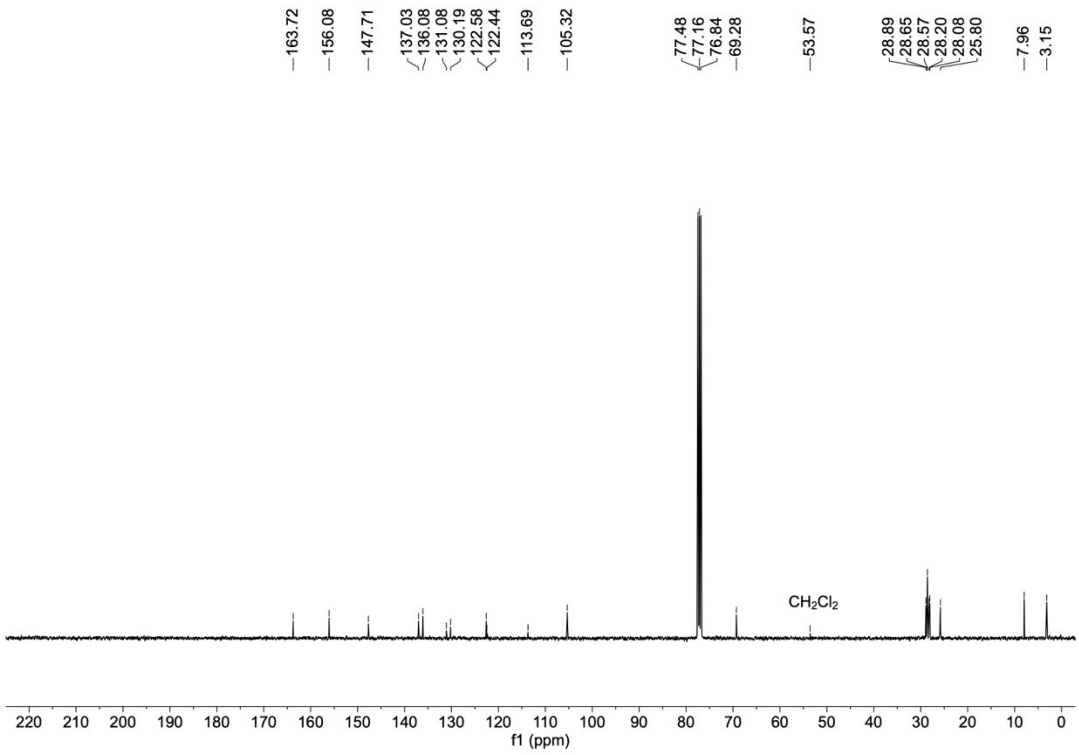

Figure S6. ^{13}C NMR spectrum of **Cycle-PBI-2Si** in $CDCl_3$.

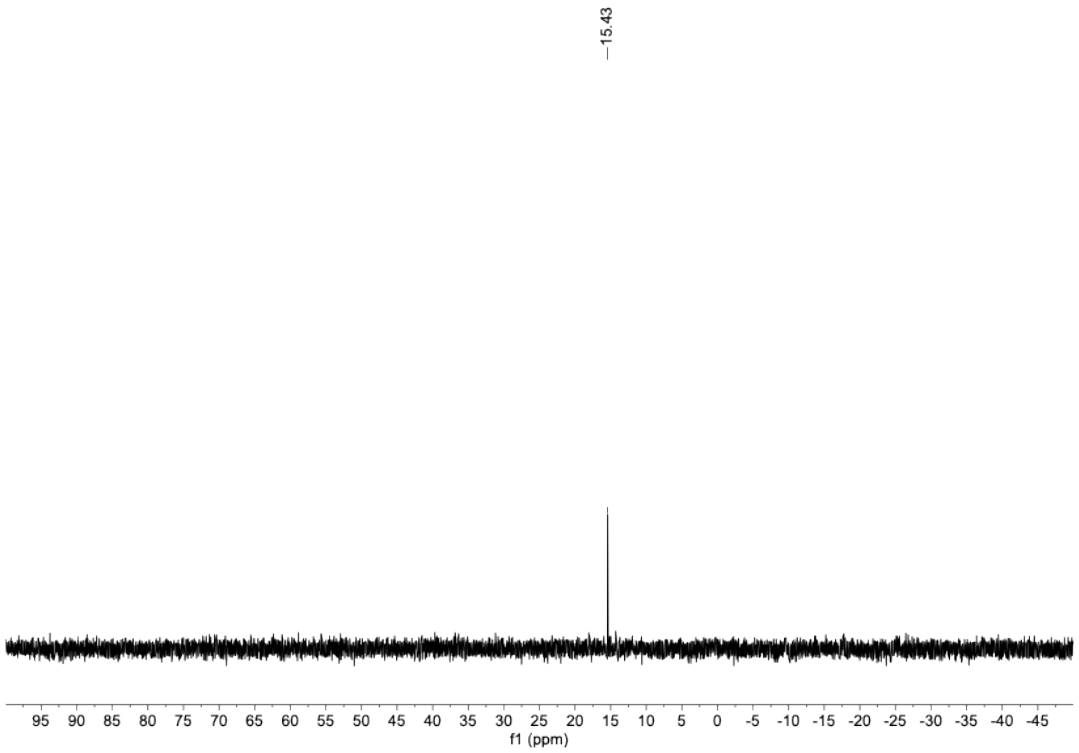

Figure S7. ^{29}Si NMR spectrum of **Cycle-PBI-2Si** in $CDCl_3$.

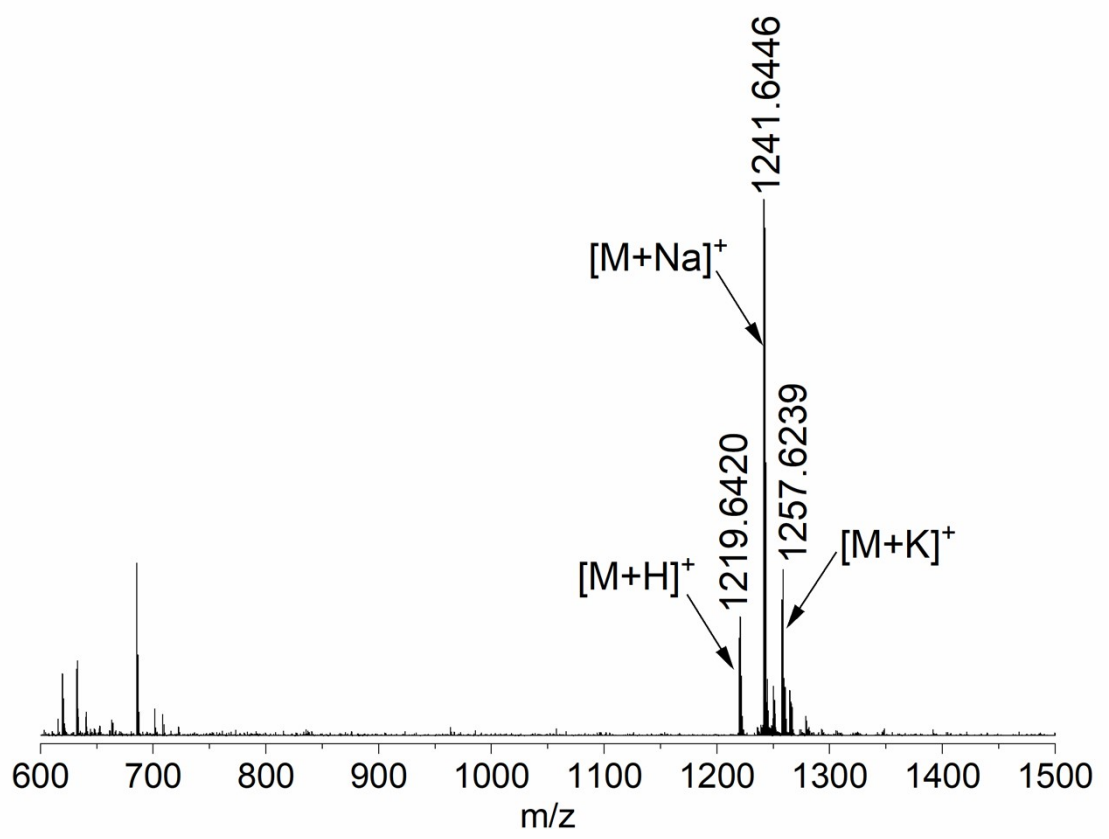

Figure S8. MALDI-TOF mass spectrum of **Cycle-PBI-2Si**.

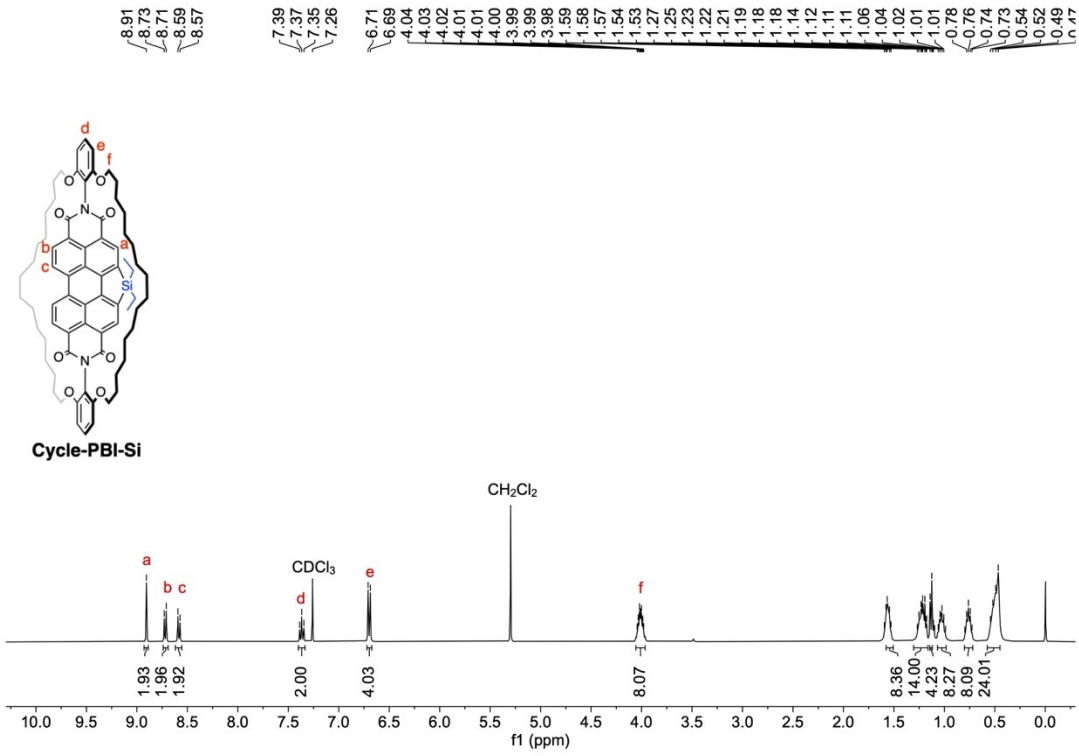

Figure S9. ^{1}H NMR spectrum of **Cycle-PBI-Si** in $CDCl_3$.

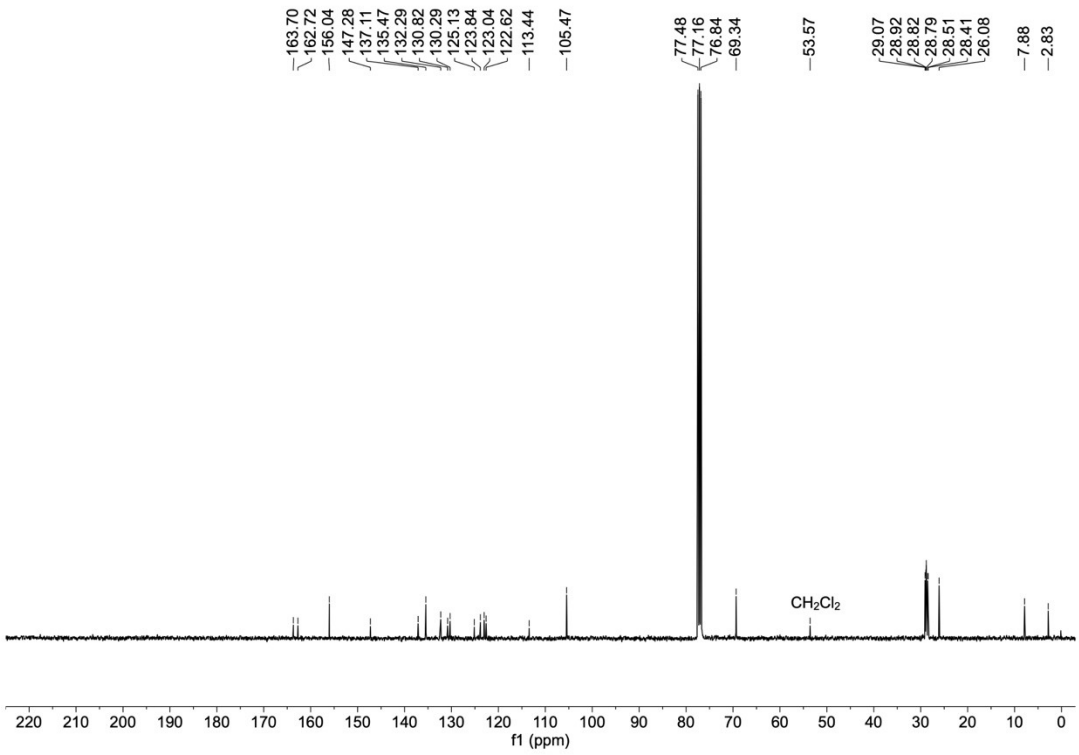

Figure S10. ^{13}C NMR spectrum of **Cycle-PBI-Si** in $CDCl_3$.

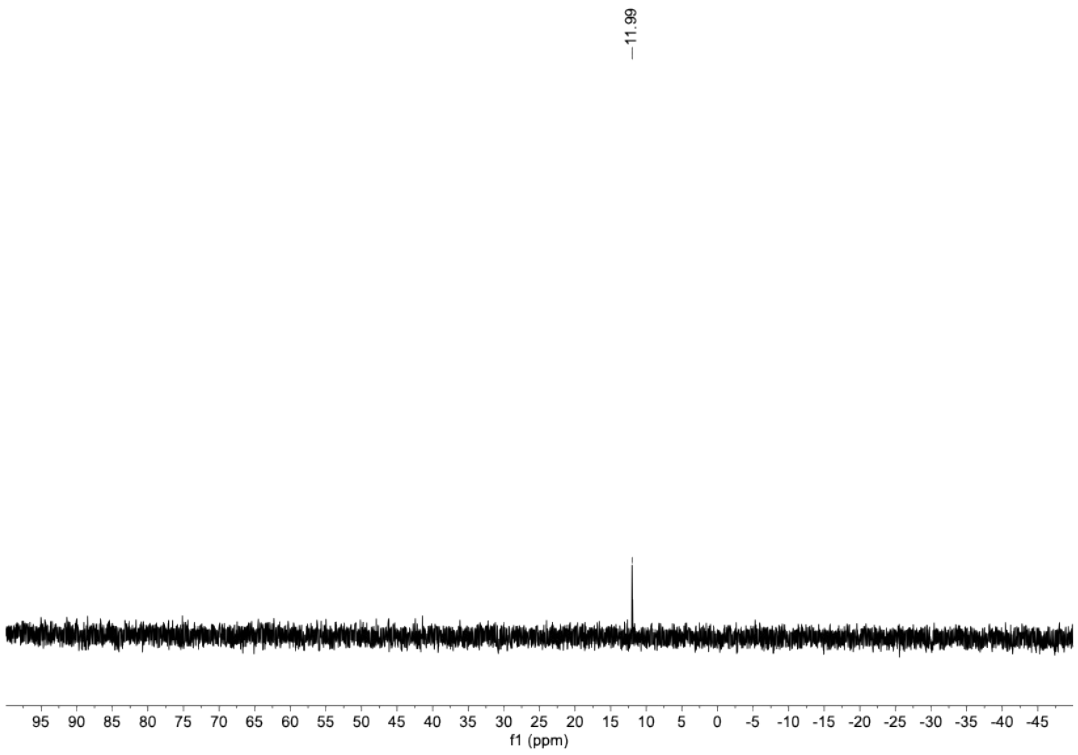

Figure S11. ^{29}Si NMR spectrum of **Cycle-PBI-Si** in $CDCl_3$.

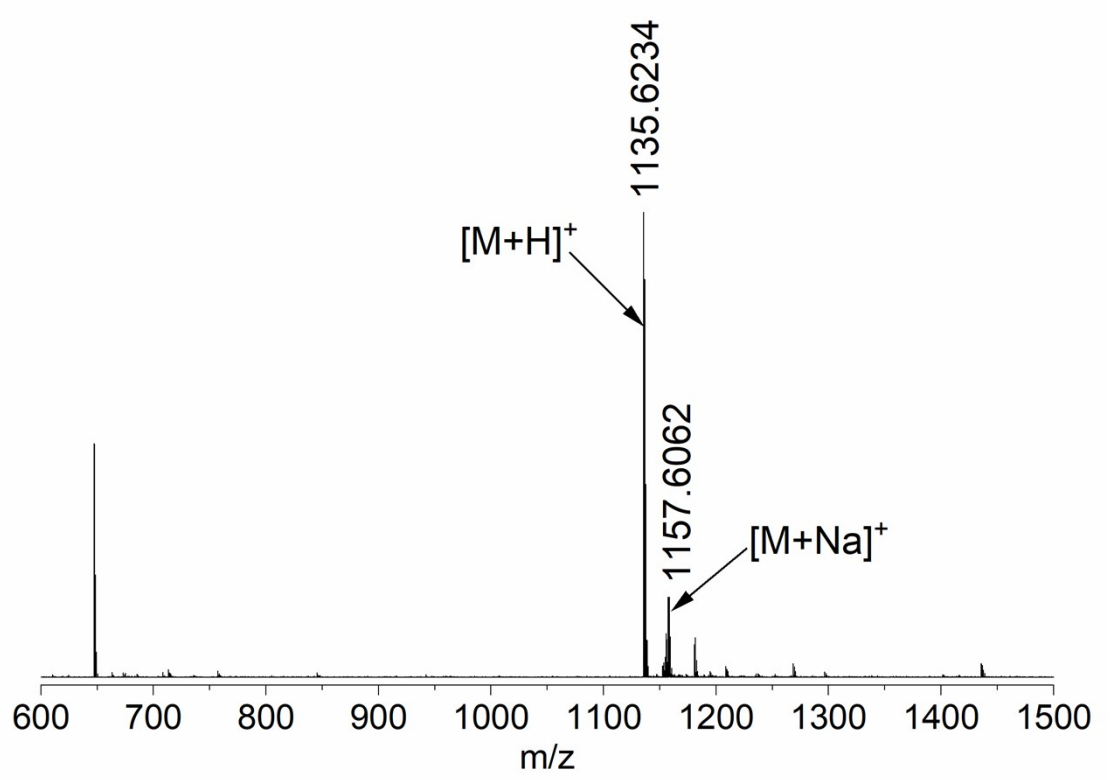

Figure S12. MALDI-TOF mass spectrum of **Cycle-PBI-Si**.

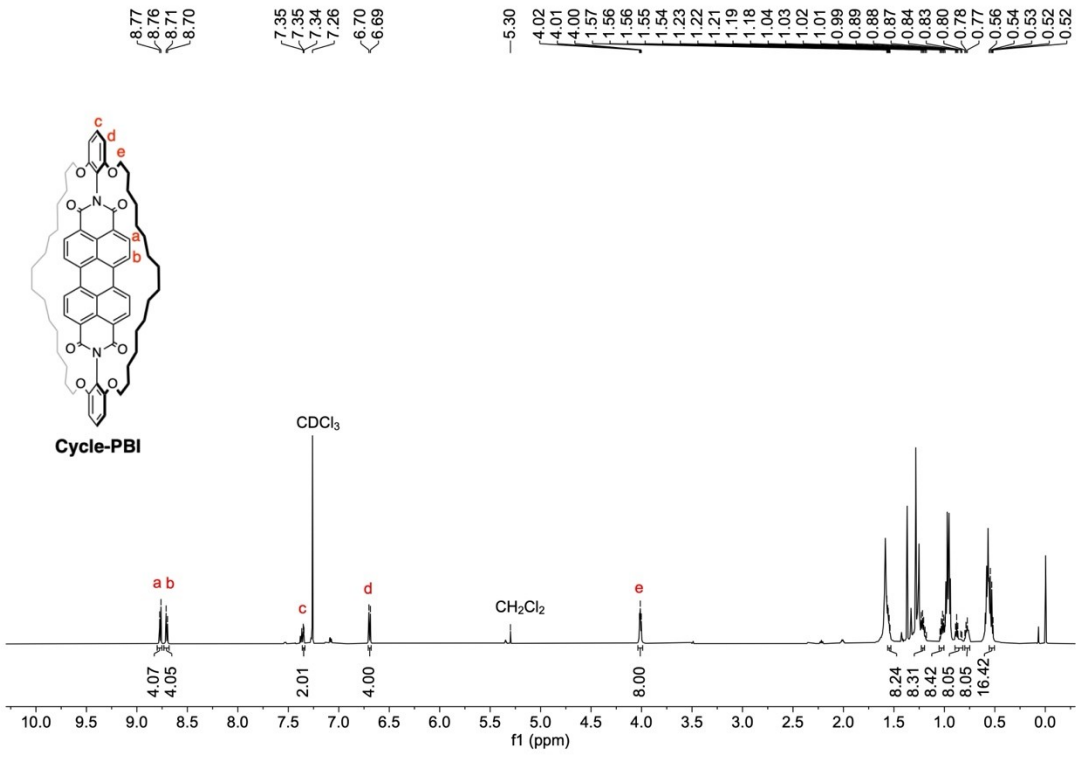

Figure S13. ^{1}H NMR spectrum of **Cycle-PBI** in $CDCl_3$.

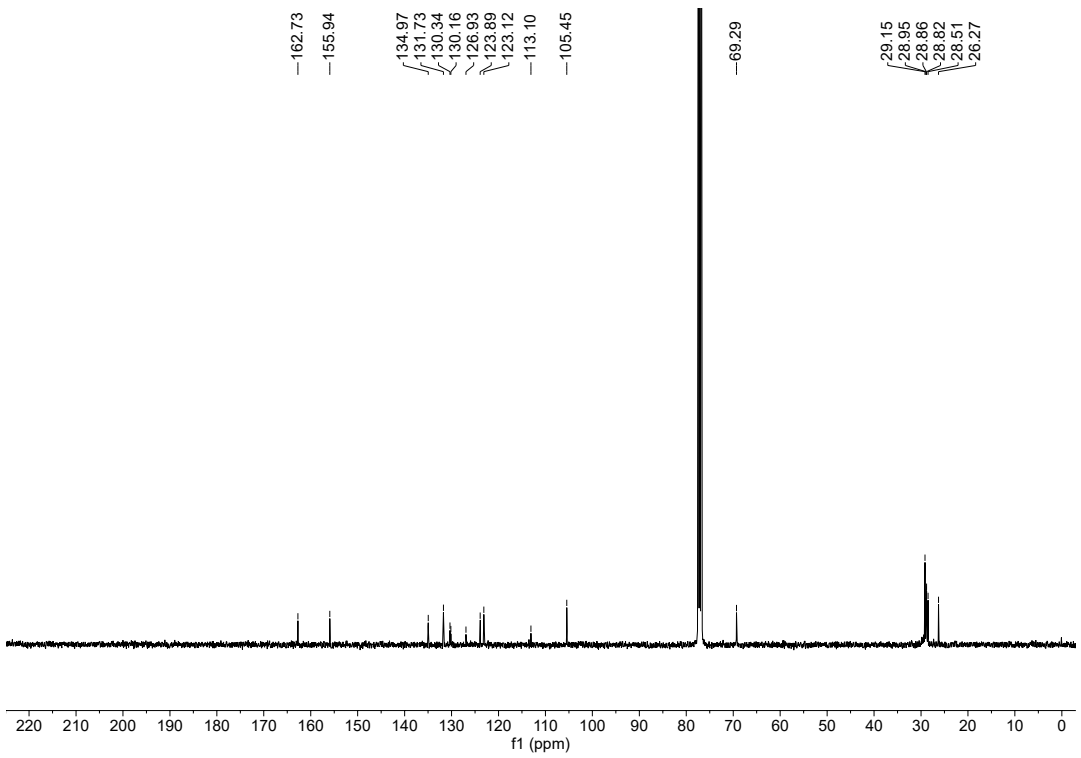

Figure S14. ^{13}C NMR spectrum of **Cycle-PBI** in $CDCl_3$.

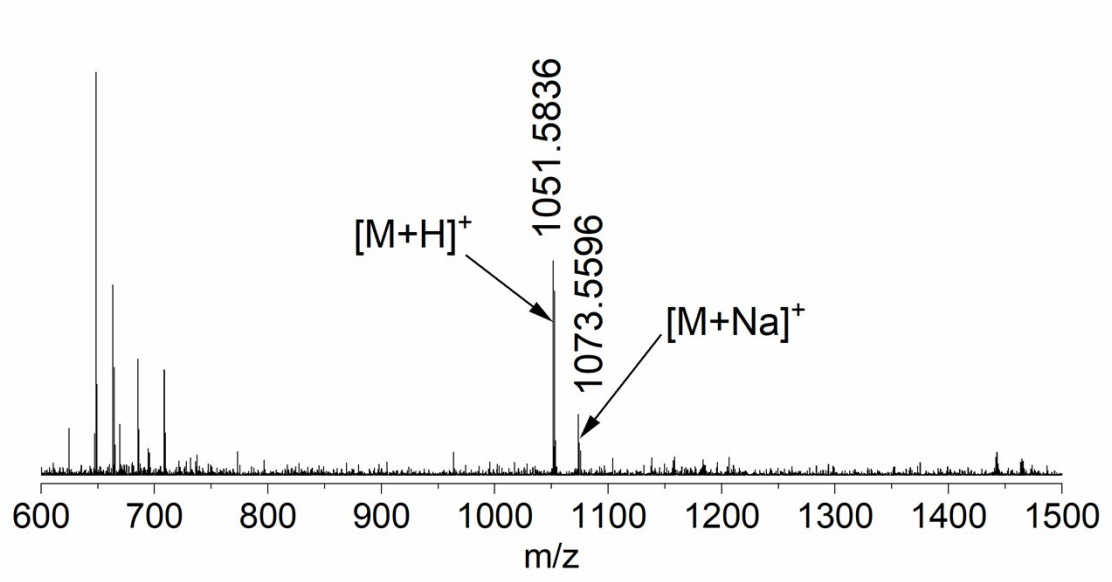

Figure S15. MALDI-TOF mass spectrum of **Cycle-PBI**.

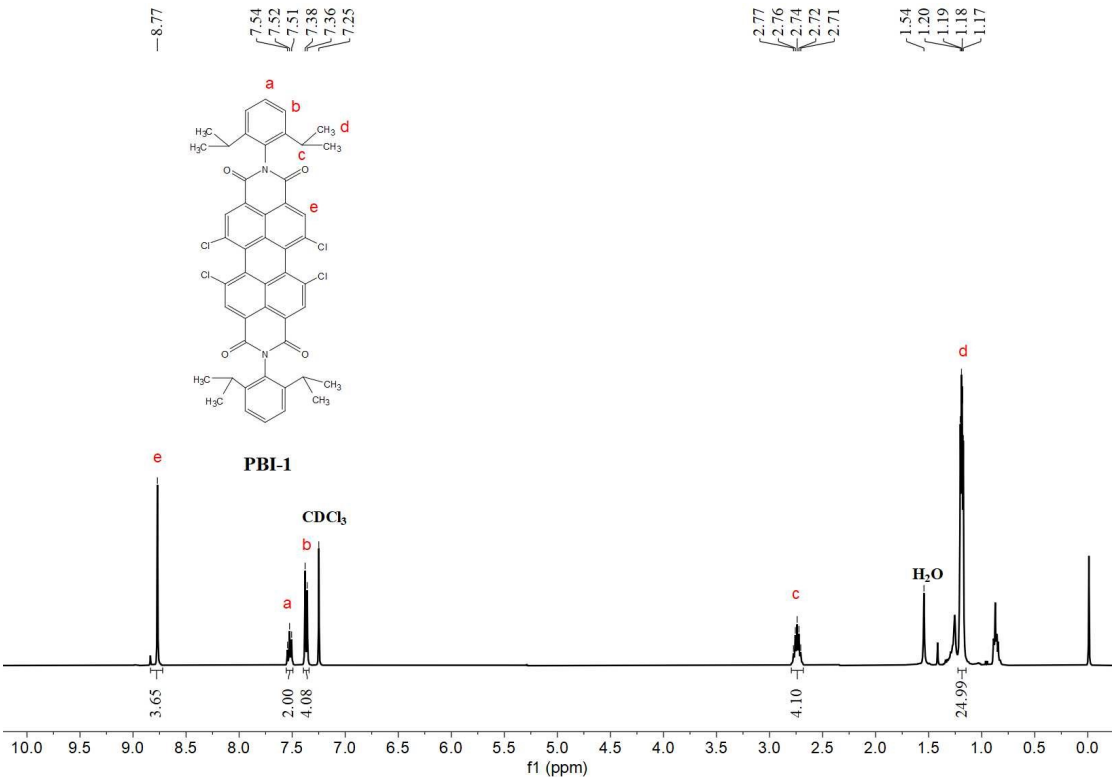

Figure S16. ^{1}H NMR spectrum of **PBI-1** in $CDCl_3$.

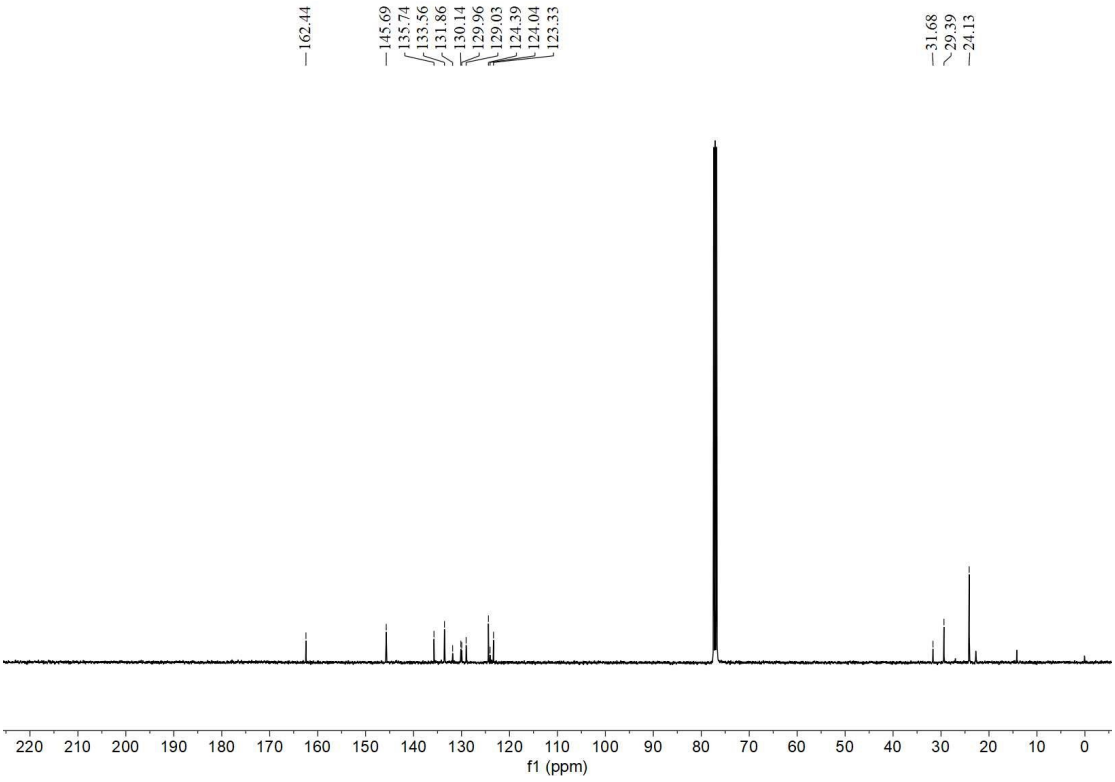

Figure S17. ^{13}C NMR spectrum of **PBI-1** in $CDCl_3$.

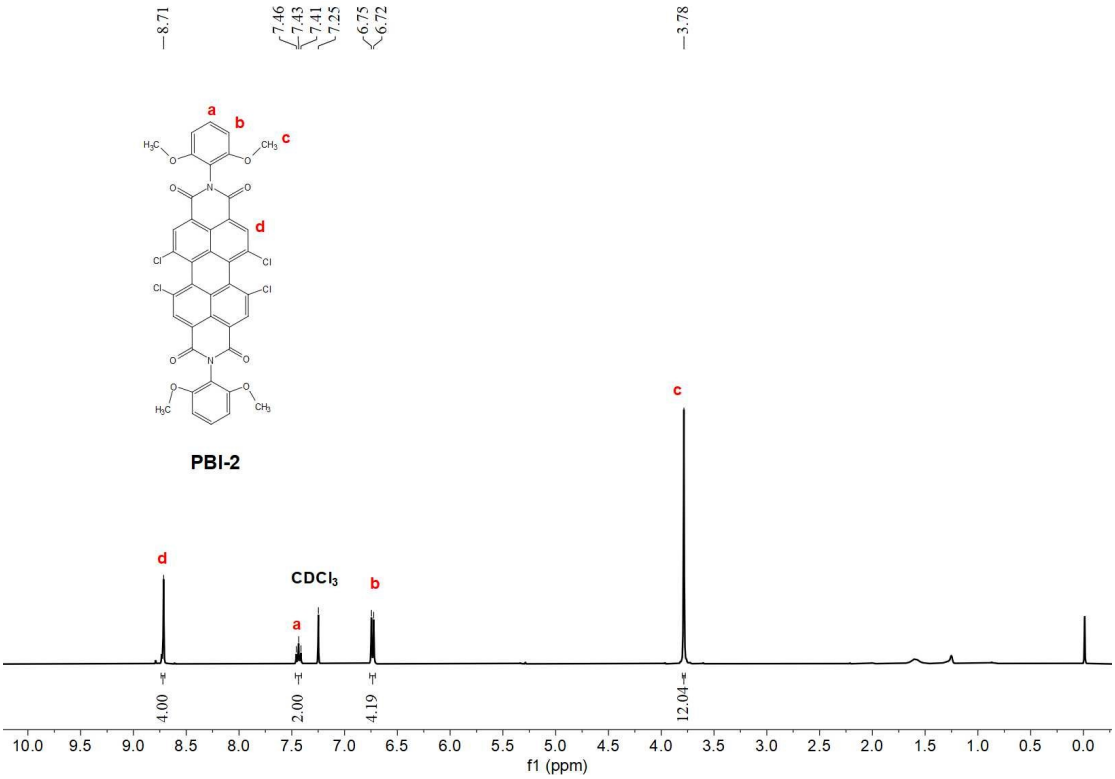

Figure S18. ^{1}H NMR spectrum of **PBI-2** in $CDCl_3$.

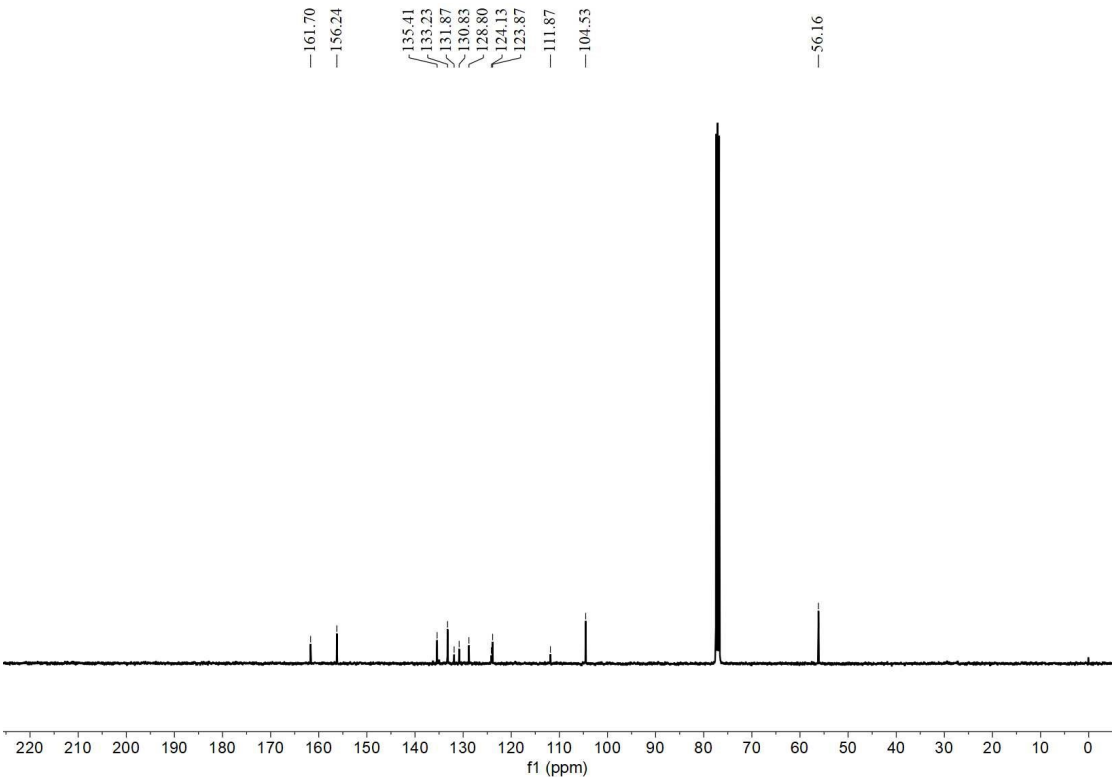

Figure S19. ^{13}C NMR spectrum of **PBI-2** in $CDCl_3$.

4. TGA Curves

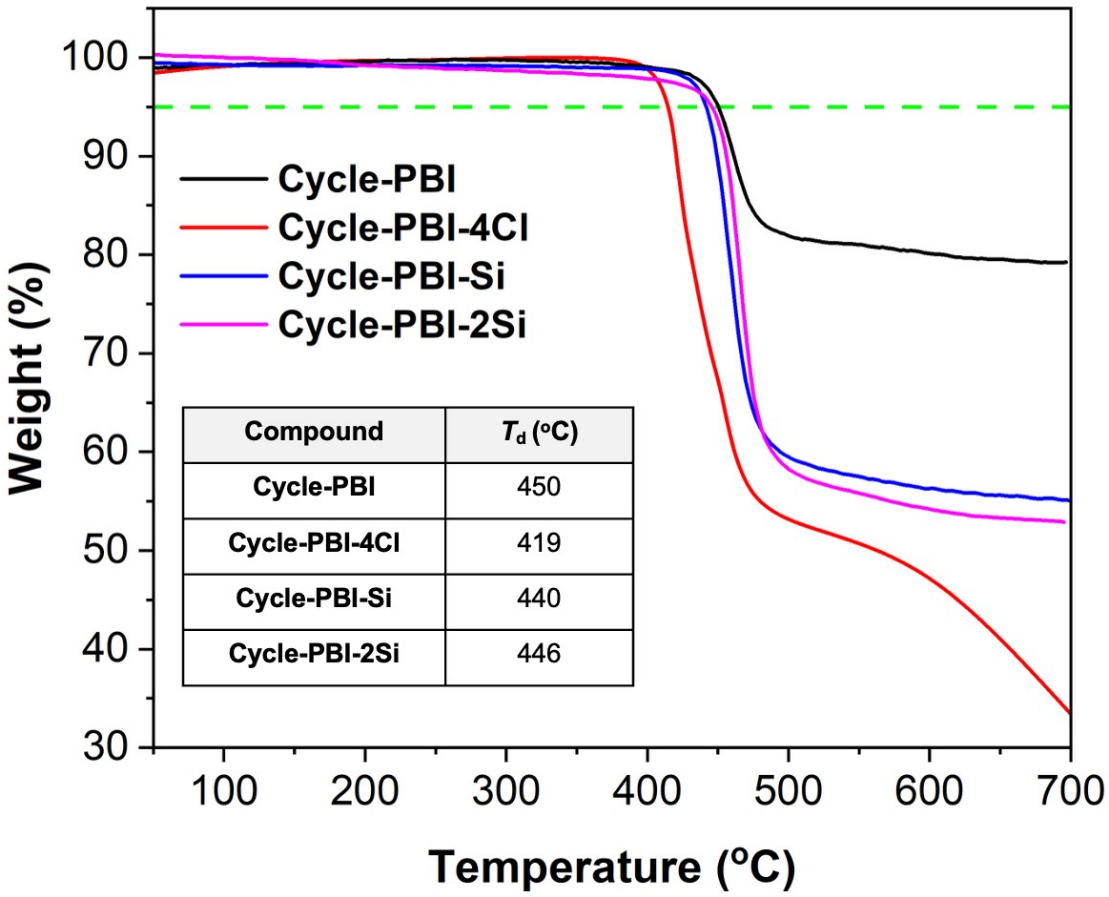

Figure S20. TGA curves for the encapsulated PBI derivatives recorded under an N_2 atmosphere at a heating rate of 10 °C min^{-1}.

5. X-ray Experimental

Diffraction grade single crystals of compound **1** were obtained by slow diffusion of hexane vapor into a tetrahydrofuran solution of compound **1**.

Diffraction grade single crystals of **Cycle-PBI** were obtained by slow diffusion of methanol vapor into a chloroform solution of **Cycle-PBI**.

Diffraction grade single crystals of **Cycle-PBI-4Cl** were obtained by slow diffusion of methanol vapor into a dichloromethane solution of **Cycle-PBI-4Cl**.

Diffraction grade single crystals of **Cycle-PBI-2Si** were obtained by slow diffusion of methanol vapor into a chloroform solution of **Cycle-PBI-2Si**.

A suitable crystal was selected, and the data were collected on a Bruker D8 Venture diffractometer using a μ-focus Cu Kα radiation source (λ = 1.54178 Å) or GaKα (λ = 1.34139 Å) with collimating mirror monochromators. Data were collected using ω-scans. The structures were solved by direct methods using SHELXT and refined by full-matrix least-squares on F^2 with anisotropic displacement parameters for the non-H atoms using SHELXL-2018/3. Structure analysis was aided by use of the programs PLATON and OLEX2.

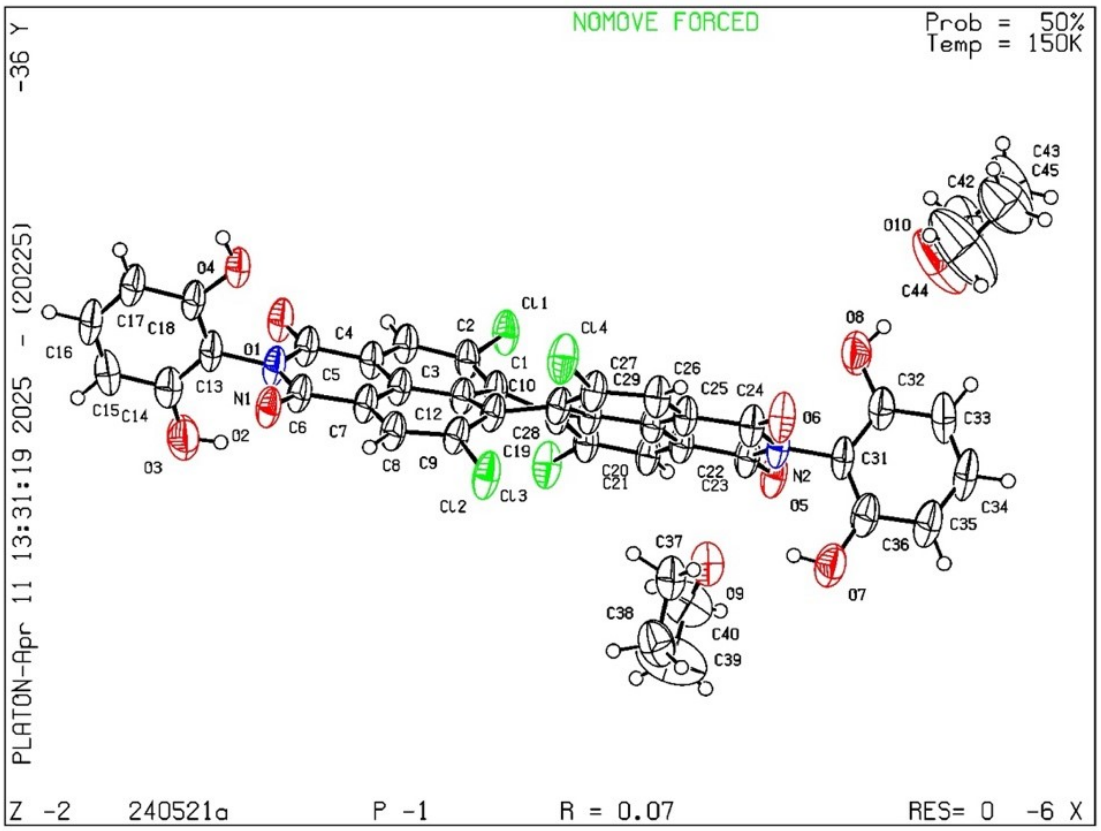

Figure S21. ORTEP drawing of **1** with the thermal ellipsoids shown at a 50% probability, which contains two tetrahydrofuran molecules. Color codes: N, blue; C, medium gray; H, white; O, red; and Cl, green.

Table S1. Crystal data and structure refinement for compound **1**.

Empirical formula	$C_{44}H_{30}Cl_4N_2O_{10}$
Formula weight	888.50
Temperature/K	150.00
Crystal system	Triclinic
Space group	P-1
a/Å	12.1193(6)
b/Å	13.7581(11)
c/Å	15.4467(10)
α/°	76.426(5)
β/°	88.096(4)
γ/°	70.477(4)
Volume/Å^3	2356.8(3)
Z	2
ρ_{calc}g/cm^3	1.252
μ/mm^{-1}	2.743
F(000)	912
Crystal size/mm^3	0.06 × 0.08 × 0.30
Radiation	CuKα (λ = 1.54178 Å)
2θ range for data collection/°	3.51 to 67.07
Index ranges	-14 ≤ h ≤ 10, -16 ≤ k ≤ 16, -18 ≤ l ≤ 18
Reflections collected	34897
Independent reflections	8359 [R_{int} = 0.0965]
Data/restraints/parameters	8359 / 0 / 542
Goodness-of-fit on F^2	1.069
Final R indexes [I>=2σ (I)]	R_1 = 0.0663, wR_2 = 0.1855
Final R indexes [all data]	R_1 = 0.0923, wR_2 = 0.2032
Largest diff. peak/hole / e Å^{-3}	0.599/-0.323
CCDC number	2464307

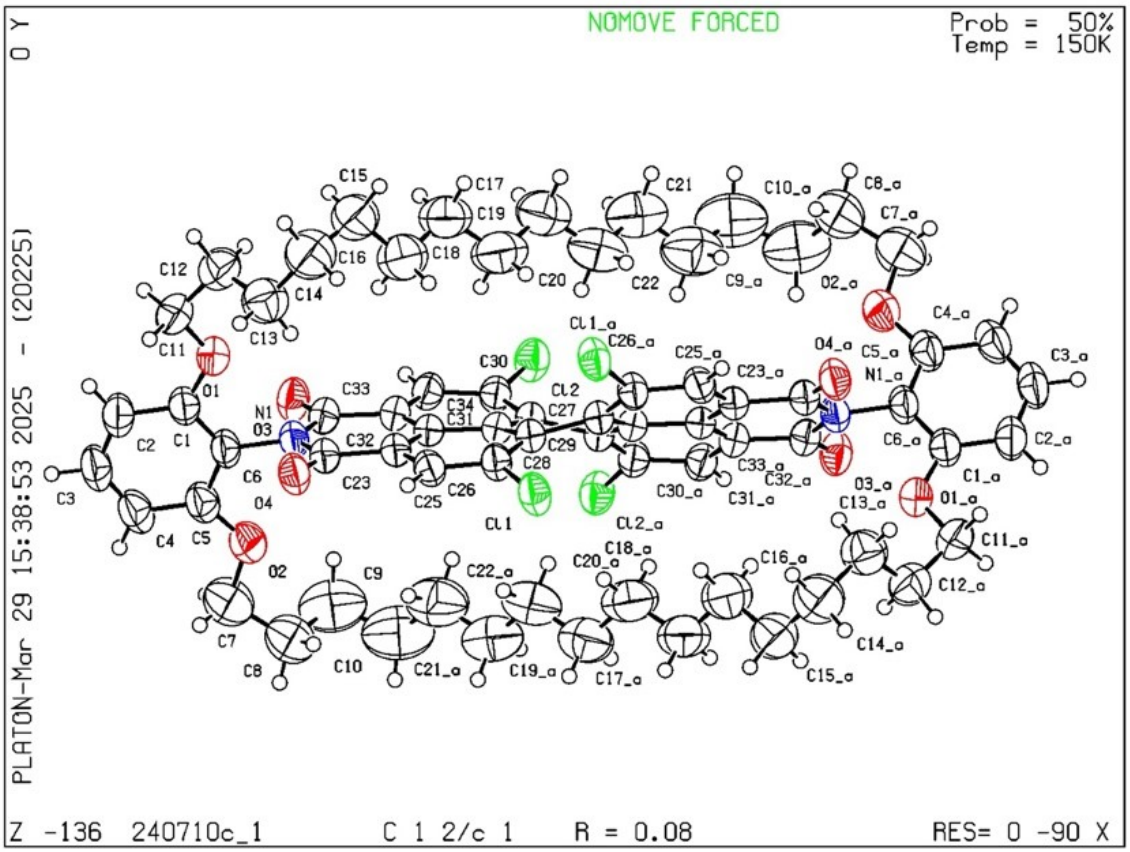

Figure S22. ORTEP drawing of **Cycle-PBI-4Cl** with the thermal ellipsoids shown at a 50% probability. Color codes: N, blue; C, medium gray; H, white; O, red; and Cl, green.

Table S2. Crystal data and structure refinement for **Cycle-PBI-4Cl**.

Empirical formula	$C_{68}H_{74}Cl_4N_2O_8$
Formula weight	1189.09
Temperature/K	150.00
Crystal system	monoclinic
Space group	C2/c
a/Å	23.6362(13)
b/Å	13.9371(9)
c/Å	19.8379(11)
α/°	90
β/°	107.054(4)
γ/°	90
Volume/Å^3	6247.6(6)
Z	4
ρ_{calc}g/cm^3	1.264
μ/mm^{-1}	2.170
F(000)	2512.0

Crystal size/mm^3	0.32 × 0.07 × 0.03
Radiation	Cu Kα (λ = 1.54178)
2θ range for data collection/°	7.452 to 133.61
Index ranges	-22 ≤ h ≤ 28, -16 ≤ k ≤ 16, -23 ≤ l ≤ 23
Reflections collected	37981
Independent reflections	5544 [R_{int} = 0.1132, R_{sigma} = 0.0683]
Data/restraints/parameters	5544/0/365
Goodness-of-fit on F^2	1.026
Final R indexes [I>=2σ (I)]	R_1 = 0.0764, wR_2 = 0.2083
Final R indexes [all data]	R_1 = 0.0999, wR_2 = 0.2349
Largest diff. peak/hole / e Å^{-3}	0.52/-0.40
CCDC number	2464308

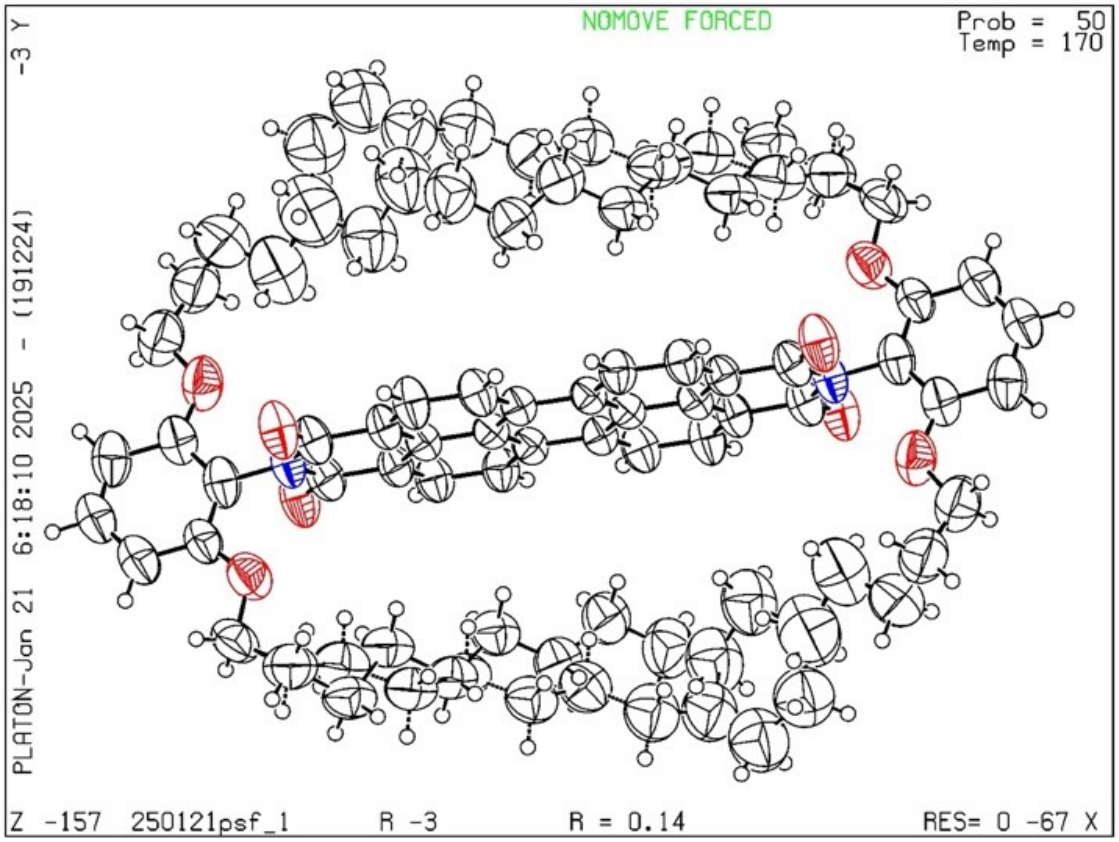

Figure S23. ORTEP drawing of **Cycle-PBI** with the thermal ellipsoids shown at a 50% probability, which shows structural disorder in the encapsulating straps. Color codes: N, blue; C, medium gray; H, white; and O, red.

Table S3. Crystal data and structure refinement for **Cycle-PBI**.

Empirical formula	$C_{68}H_{78}N_2O_8$
Formula weight	1051.32
Temperature/K	170.00

Crystal system	Trigonal
Space group	R-3
a/Å	37.0034(16)
b/Å	37.0034(16)
c/Å	11.7641(7)
α/°	90
β/°	90
γ/°	120
Volume/Å^3	13949.9(15)
Z	9
ρ_{calc}g/cm^3	1.126
μ/mm^{-1}	0.368
F(000)	5076
Crystal size/mm^3	0.17 × 0.17 × 0.05
Radiation	Ga Kα (λ = 1.34139 Å)
2θ range for data collection/°	6.964 to 110.41
Index ranges	-43 ≤ h ≤ 45, -45 ≤ k ≤ 44, -14 ≤ l ≤ 14
Reflections collected	45893
Independent reflections	5882 [R_{int} = 0.0909]
Data/restraints/parameters	5882 / 263 / 434
Goodness-of-fit on F^2	1.101
Final R indexes [I>=2σ (I)]	R_1 = 0.1355, wR_2 = 0.2924
Final R indexes [all data]	R_1 = 0.1707, wR_2 = 0.3106
Largest diff. peak/hole / e Å^{-3}	0.43/-0.40
CCDC number	2464309

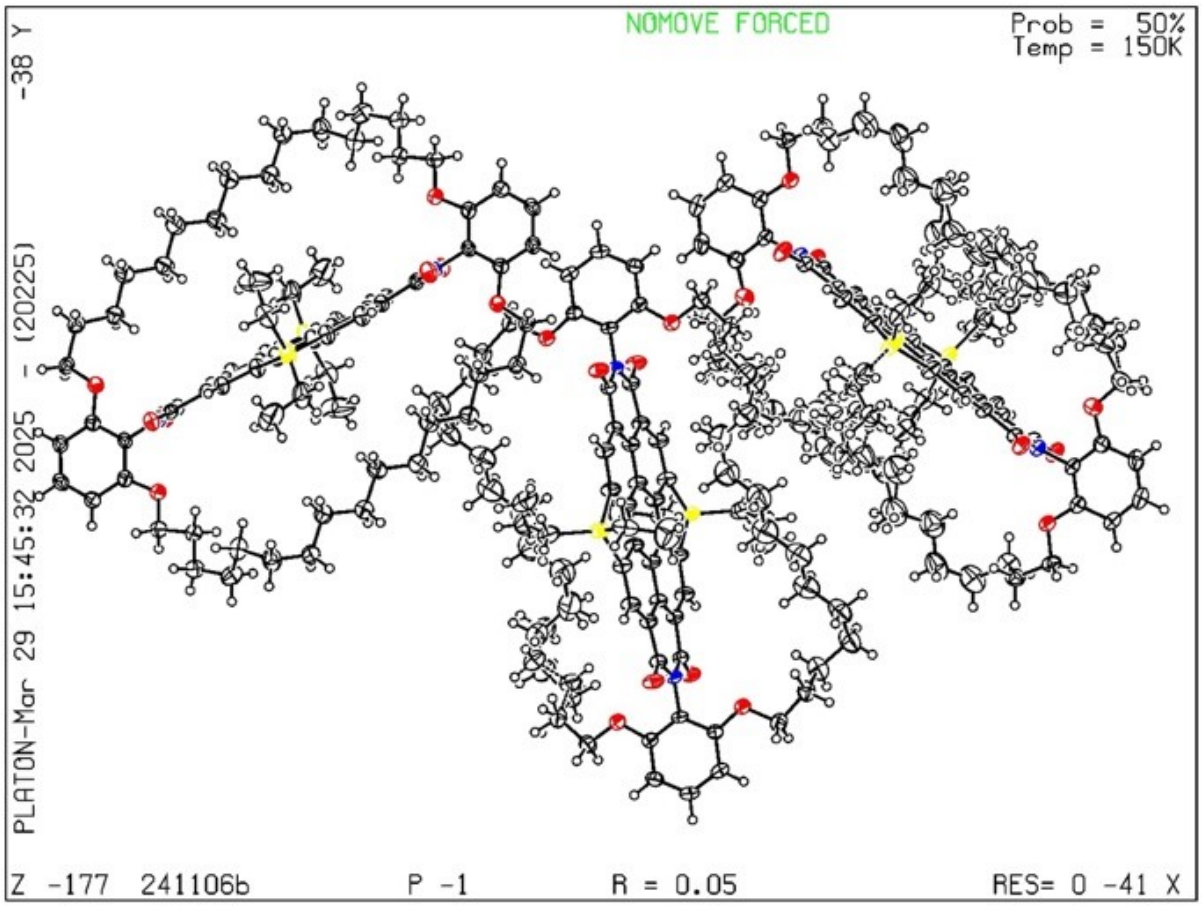

Figure S24. ORTEP drawing of **Cycle-PBI-2Si** with the thermal ellipsoids shown at a 50% probability, which contains three molecules in the unit cell and shows structural disorder in the ethyl chains and the encapsulating straps. Color codes: N, blue; C, medium gray; H, white; O, red; and Si, yellow.

Table S4. Crystal data and structure refinement for **Cycle-PBI-2Si**.

Empirical formula	$C_{76}H_{94}N_2O_8Si_2$
Formula weight	1219.71
Temperature/K	150.00
Crystal system	triclinic
Space group	P-1
a/Å	14.3403(15)
b/Å	17.3349(19)
c/Å	21.378(2)
α/°	81.643(6)
β/°	79.108(6)
γ/°	87.491(6)

Volume/Å^3	5162.4(10)
Z	3
ρ_{calc}g/cm^3	1.177
μ/mm^{-1}	0.907
F(000)	1968.0
Crystal size/mm^3	0.2 × 0.18 × 0.03
Radiation	Cu Kα (λ = 1.54178)
2θ range for data collection/°	4.25 to 118.25
Index ranges	-15 ≤ h ≤ 15, -19 ≤ k ≤ 19, -23 ≤ l ≤ 23
Reflections collected	93305
Independent reflections	14834 [R_{int} = 0.0968, R_{sigma} = 0.0595]
Data/restraints/parameters	14834/409/1350
Goodness-of-fit on F^2	1.072
Final R indexes [I>=2σ (I)]	R_1 = 0.0511, wR_2 = 0.1383
Final R indexes [all data]	R_1 = 0.0638, wR_2 = 0.1483
Largest diff. peak/hole / e Å^{-3}	0.46/-0.45
CCDC number	2464311

6. Photophysical Properties

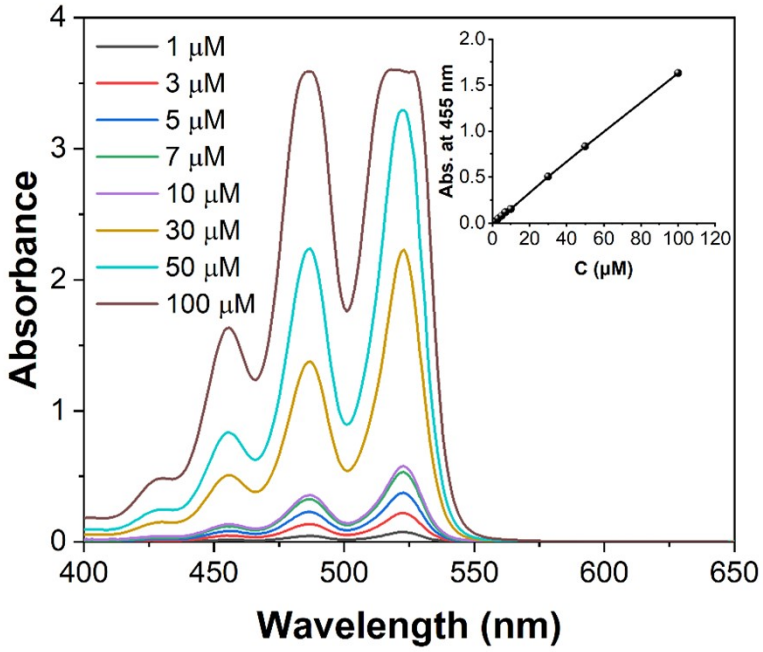

Figure S25. Concentration-dependent UV-Vis absorption spectra of **Cycle-PBI** in toluene solutions (concentration from 1×10^{-6} to 1×10^{-4} M). Inset: dependence of the absorbance intensity at 472 nm on the concentration.

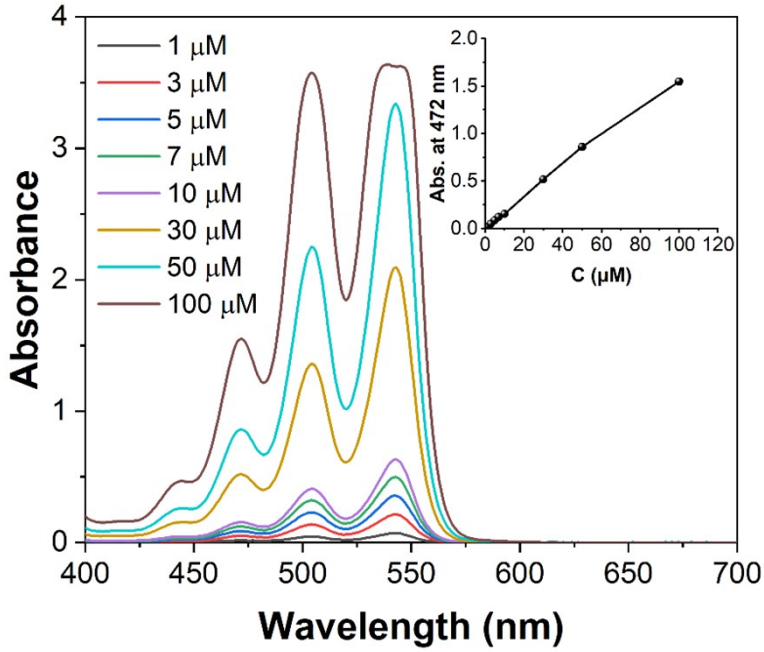

Figure S26. Concentration-dependent UV-Vis absorption spectra of **Cycle-PBI-Si** in toluene solutions (concentration from 1×10^{-6} to 1×10^{-4} M). Inset: dependence of the absorbance intensity at 472 nm on the concentration.

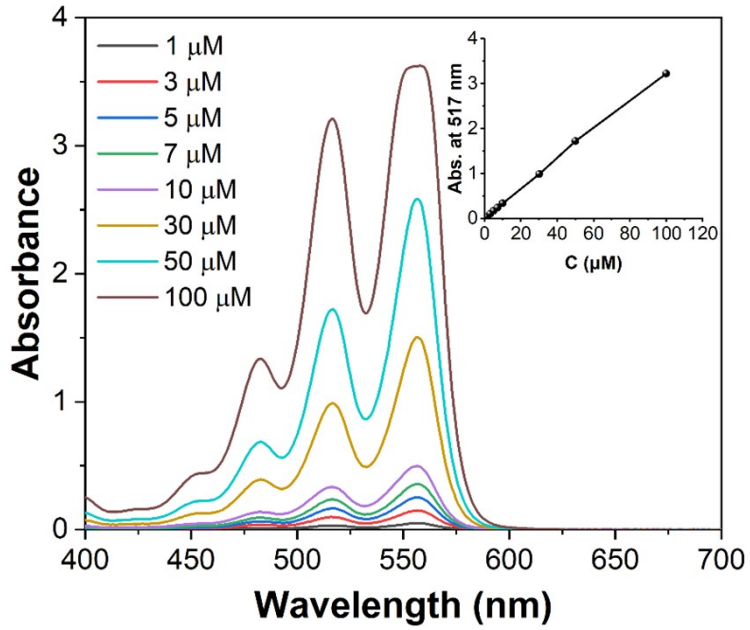

Figure S27. Concentration-dependent UV-Vis absorption spectra of **Cycle-PBI-2Si** in toluene solutions (concentration from 1×10^{-6} to 1×10^{-4} M). Inset: dependence of the absorbance intensity at 517 nm on the concentration.

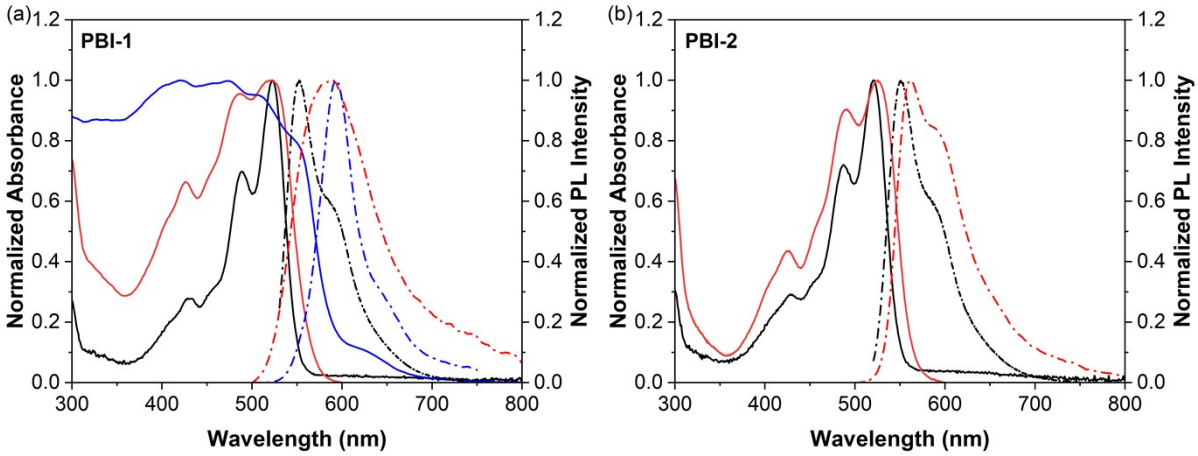

Figure S28. (a) Normalized UV-Vis absorption (solid lines) and fluorescence (dash dot lines) spectra of model compounds in dilute toluene solutions (black lines, 1×10^{-5} M for UV-Vis absorption spectra and 1×10^{-6} M for fluorescence spectra), thin films (red lines) and microcrystalline powders (blue lines): (a) **PBI-1** and (b) **PBI-2**. Notably, microcrystalline **PBI-2** powders exhibit negligible fluorescence.

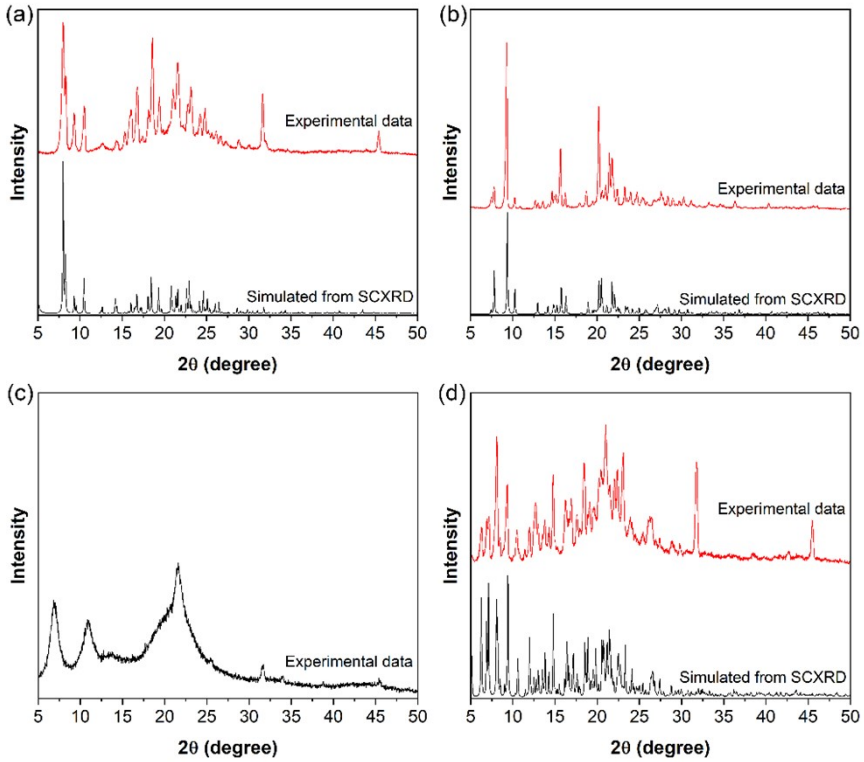

Figure S29. The experimental powder XRD patterns of **Cycle-PBI** (a), **Cycle-PBI-4Cl** (b), **Cycle-PBI-Si** (c), and **Cycle-PBI-2Si** (d) compared with simulated patterns derived from their single crystal structures.

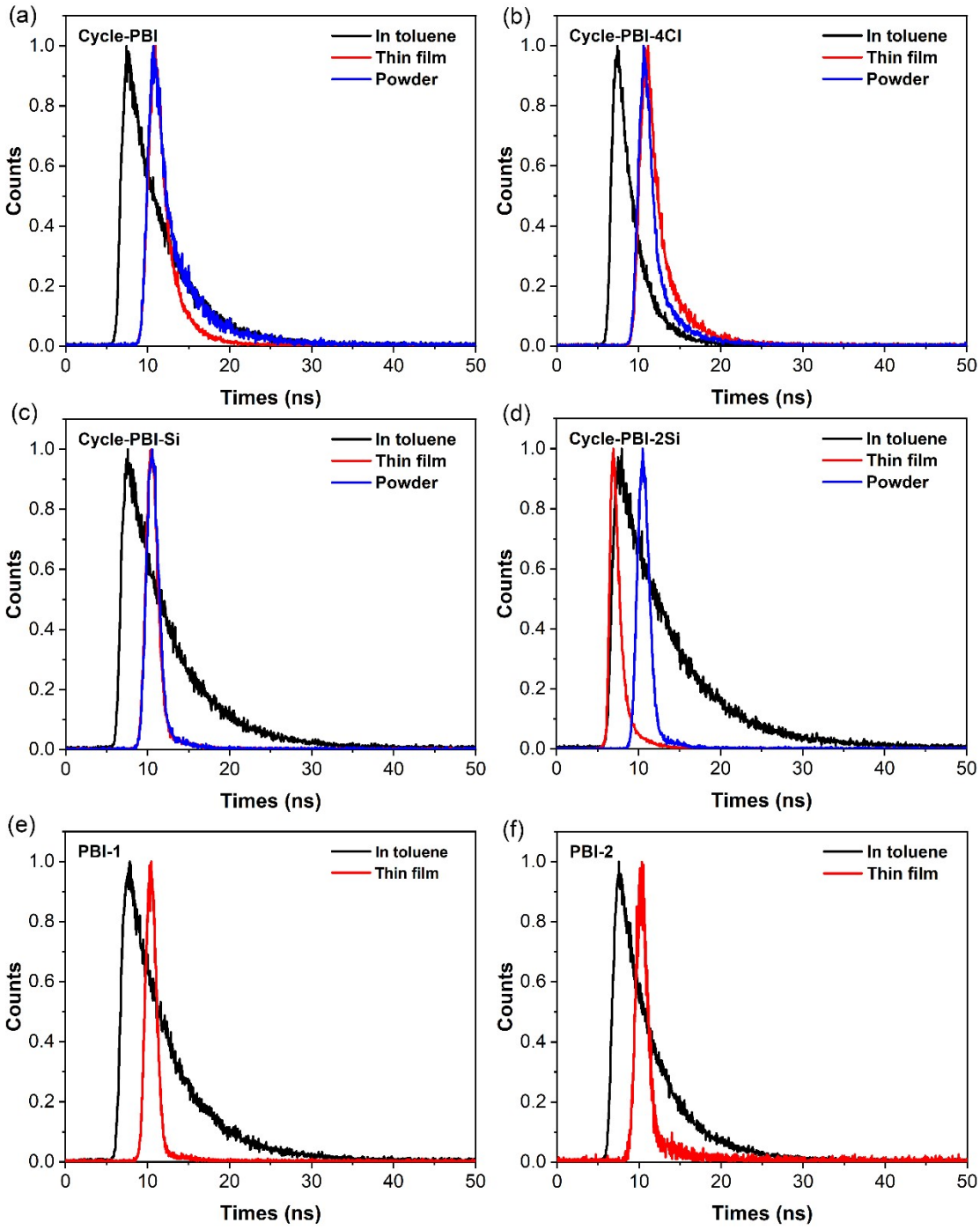

Figure S30. Time-resolved emission spectra of PBI compounds in in dilute toluene solution (1×10^{-6} M) and the solid states. Decaying lifetimes of the PBI compounds were measured at their maximum emission wavelengths.

Table S5. Electrochemical and computational data of the encapsulated PBI compounds.

	$E_{re/onset}$ (V)	$E_{ox/onset}$ (V)	LUMO [a] (eV)	HOMO [a] (eV)	E_g^{cv} [b] (eV)	LUMO [c] (eV)	HOMO [c] (eV)	E_g^{cal} [d] (eV)
Cycle-PBI	-0.79	1.36	-3.96	-6.11	2.15	-3.47	-6.01	2.54
Cycle-PBI-4Cl	-0.61	1.41	-4.14	-6.16	2.02	-3.74	-6.17	2.43
Cycle-PBI-Si	-0.81	1.32	-3.94	-6.07	2.13	-3.41	-5.9	2.49
Cycle-PBI-2Si	-0.82	1.30	-3.93	-6.05	2.12	-3.36	-5.82	2.46

[a] HOMO and LUMO energy levels were estimated from the onset oxidation and reduction potentials (vs. Ag/Ag^+) plus 4.75, respectively.

[b] $E_g^{cv} = E_{LUMO}^{cv} - E_{HOMO}^{cv}$.

[c] HOMO and LUMO energy levels calculated by DFT calculations.

[d] $E_g^{cal} = E_{LUMO}^{cv} - E_{HOMO}^{cv}$.

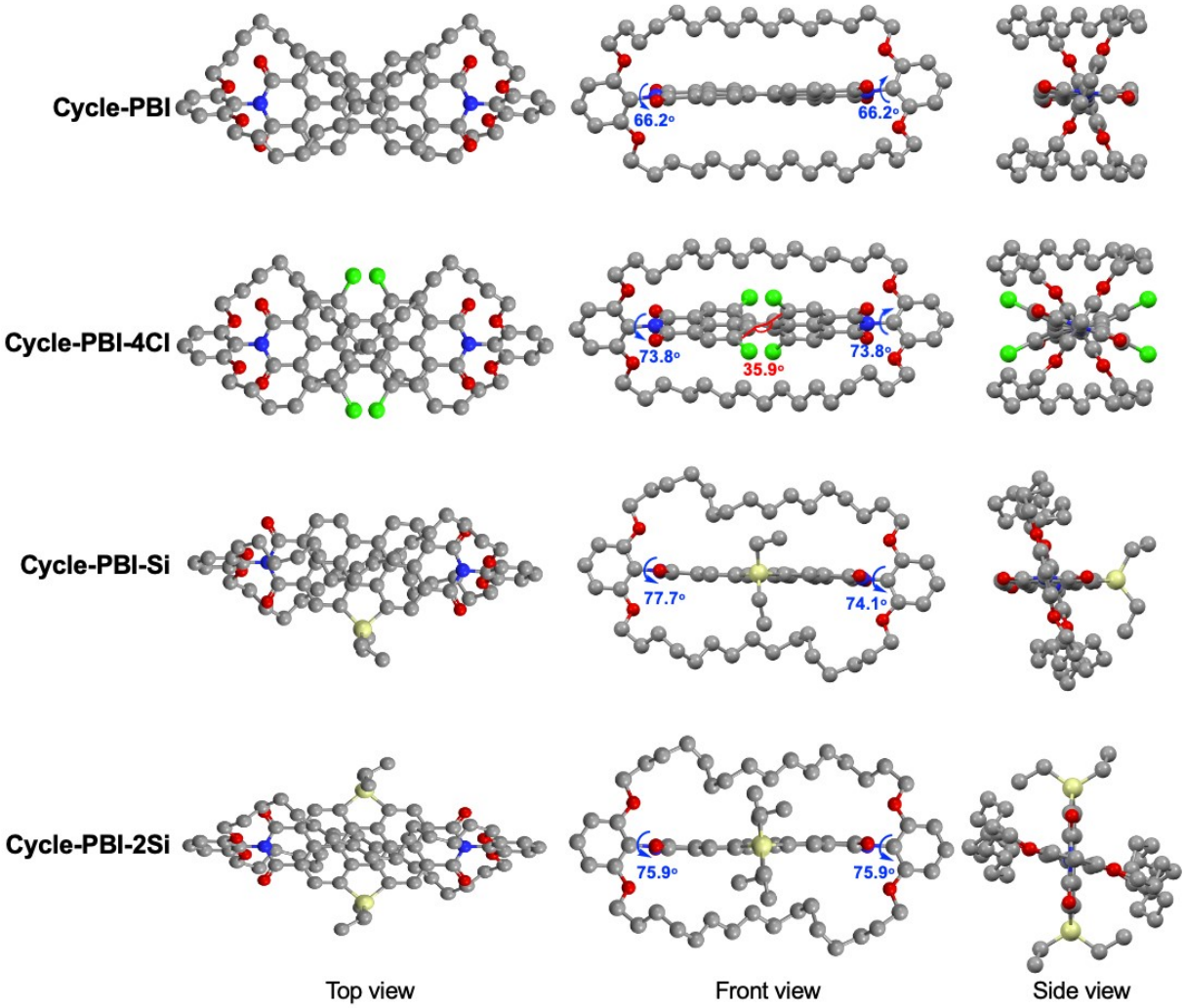

Figure S31. Optimized geometries for the doubly-strapped PBI derivatives obtained from ground-state DFT calculations at the B3LYP-D3/6-311G(d,p) level. Color codes: C (medium grey), N (blue), O (red), Cl (green), and Si (yellow). Torsion angles between the imide phenyl rings and naphthalene planes are shown in blue, and the dihedral angle of the twisted perylene backbone in **Cycle-PBI-4Cl** is indicated in red.

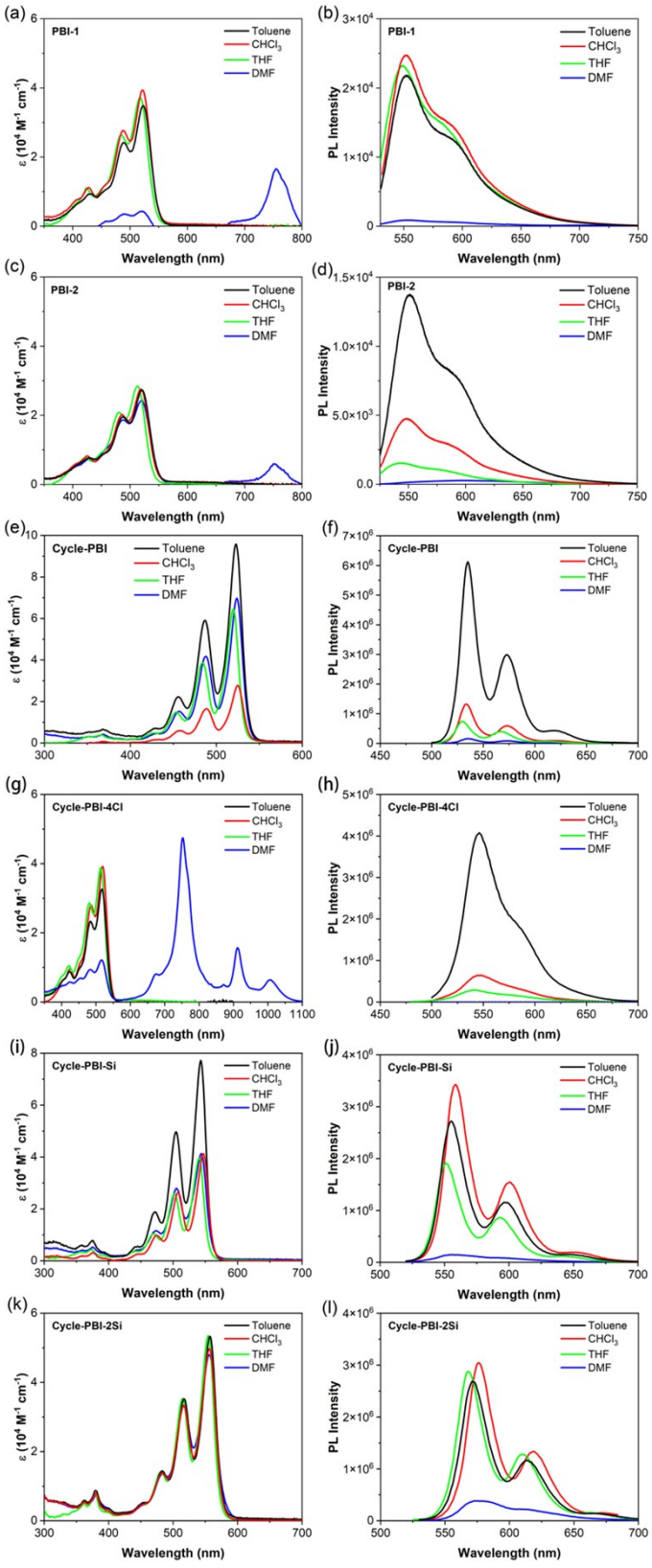

Figure S32. Absorption and fluorescence spectra of (a, b) **PBI-1**, (c, d) **PBI-2**, (e, f) **Cycle-PBI**, (g, h) **Cycle-PBI-4Cl**, (i, j) **Cycle-PBI-Si**, and (k, l) **Cycle-PBI-2Si** in variety of solvents with different polarity (1×10^{-5} M). The corresponding dielectric constants: toluene ($\varepsilon = 2.38$) < $CHCl_3$ ($\varepsilon = 4.8$) < THF ($\varepsilon = 7.52$) < DMF ($\varepsilon = 38.25$).

Table S6. Photophysical properties of the encapsulated PBI compounds in different polar solvents.

Compounds	Solvent	$\lambda_{abs,\ max}$ [a] [nm]	ε [10^4 M^{-1} cm^{-1}]	$\lambda_{em,\ max}$ [b] [nm]	Φ_F [c] [%]
Cycle-PBI	Toluene	523	6.36	535	~100
	$CHCl_3$	525	2.77	534	86.7
	THF	520	6.45	530	10.5
	DMF	524	6.97	534	2.5
Cycle-PBI-4Cl	Toluene	518	3.35	546	27.6
	$CHCl_3$	519	3.92	547	5.6
	THF	514	3.88	541	0.87
	DMF	753	4.74	-	-
Cycle-PBI-Si	Toluene	543	3.76	555	93.2
	$CHCl_3$	547	4.13	558	95.7
	THF	540	3.96	551	65.1
	DMF	544	4.13	555	10.8
Cycle-PBI-2Si	Toluene	557	5.33	571	~100
	$CHCl_3$	562	5.39	576	99.5
	THF	554	5.35	568	99.8
	DMF	556	4.8	572	20.5

[a] 1×10^{-5} M for UV-Vis absorption spectra.

[b] 1×10^{-6} M for fluorescence spectra.

[c] Measured using an integrating sphere.

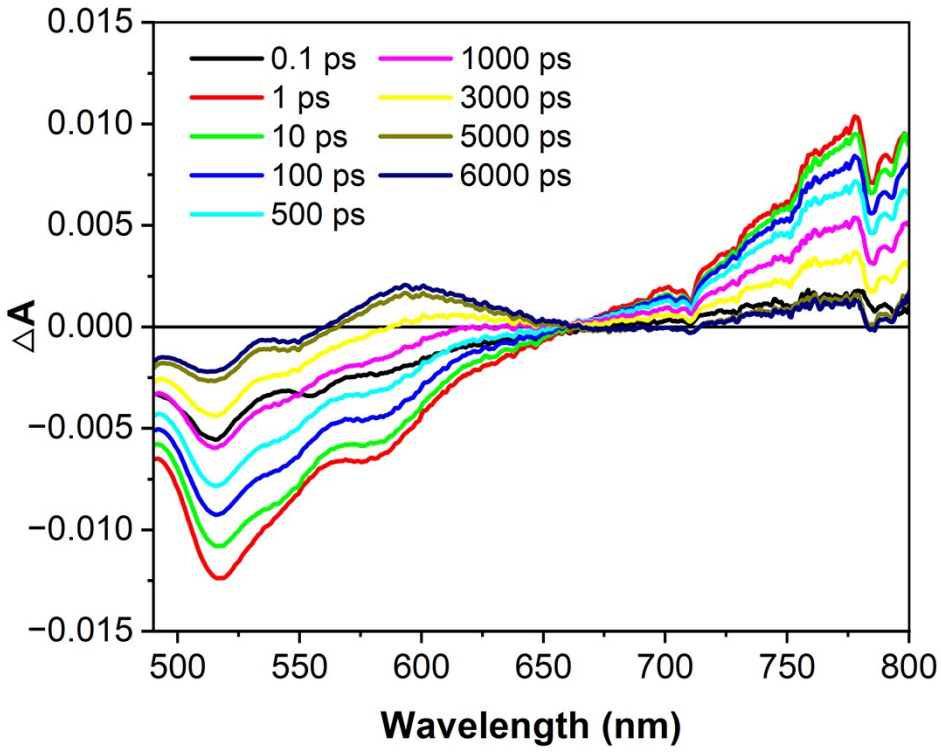

Figure S33. Femtosecond transient spectra of **PBI-2** excited at 482 nm in toluene (5×10^{-5} M) at room temperature.

7. DFT Calculations

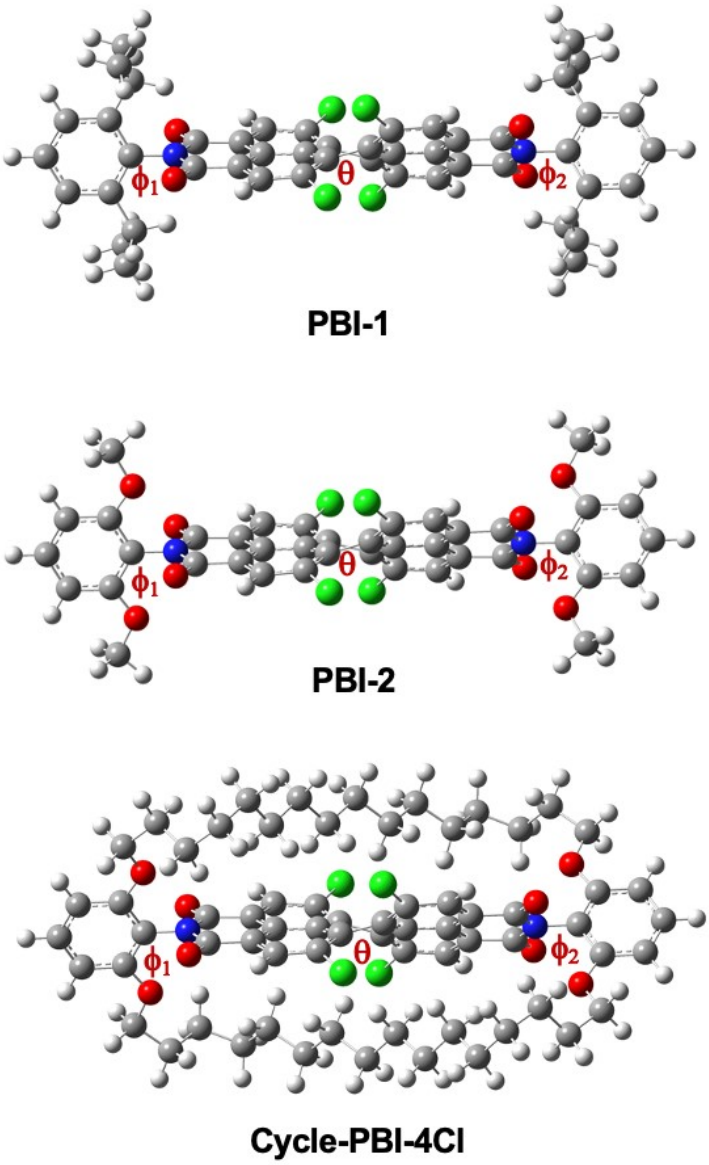

Figure S34. Optimized structures of **PBI-1**, **PBI-2** and **Cycle-PBI-4Cl** calculated at the B3LYP-D3/6-311G(d,p) level.

Table S7. The calculated torsion angles in the **PBI-1**, **PBI-2** and **Cycle-PBI-4Cl**.

	ϕ_1	ϕ_2	θ
PBI-1	87.4	87.4	35.4
PBI-2	87.2	87.2	35.4
Cycle-PBI-4Cl	75.5	76.7	35.3

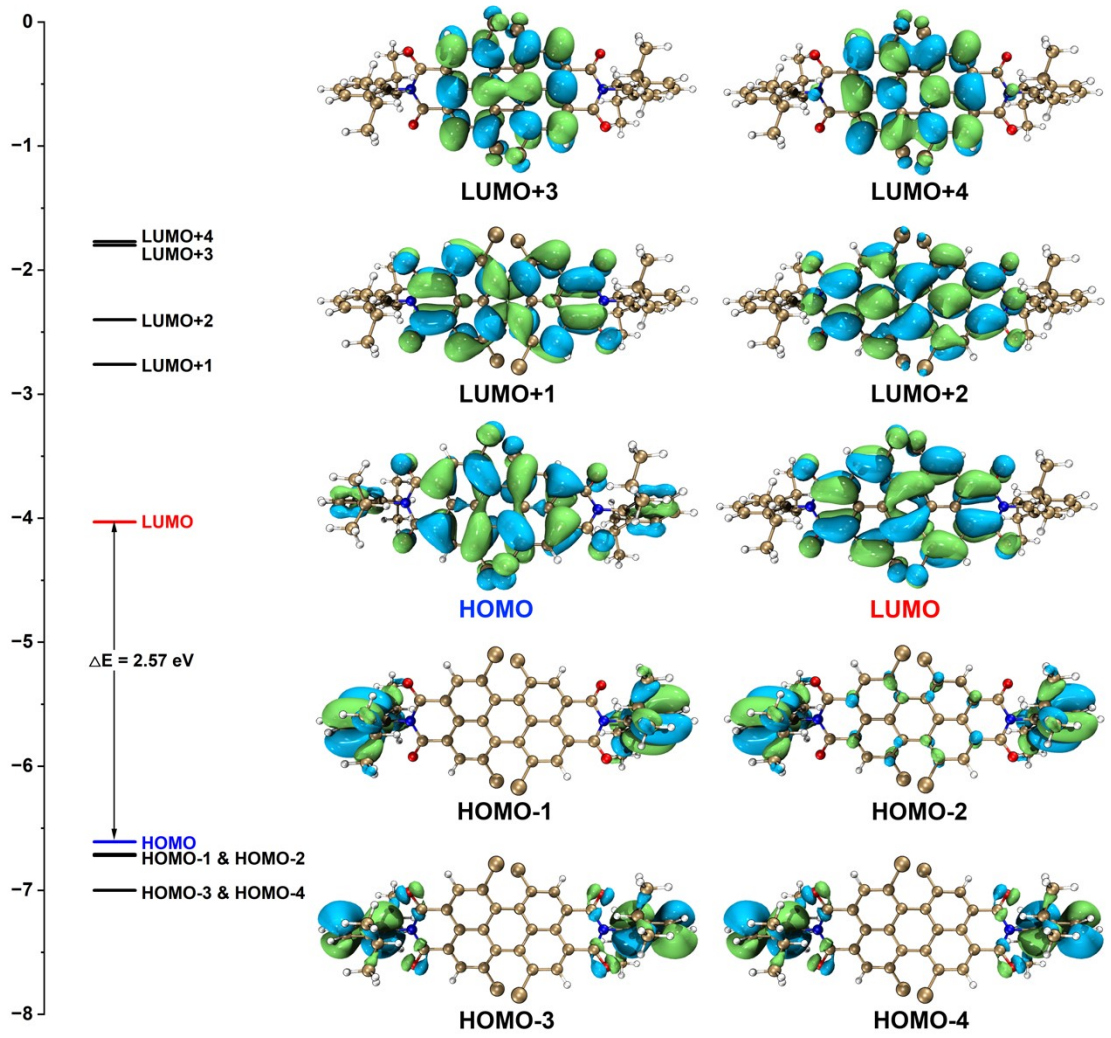

Figure S35. The MO energy diagrams and selected frontier MOs for **PBI-1** calculated at the B3LYP-D3/6-311G(d,p) level.

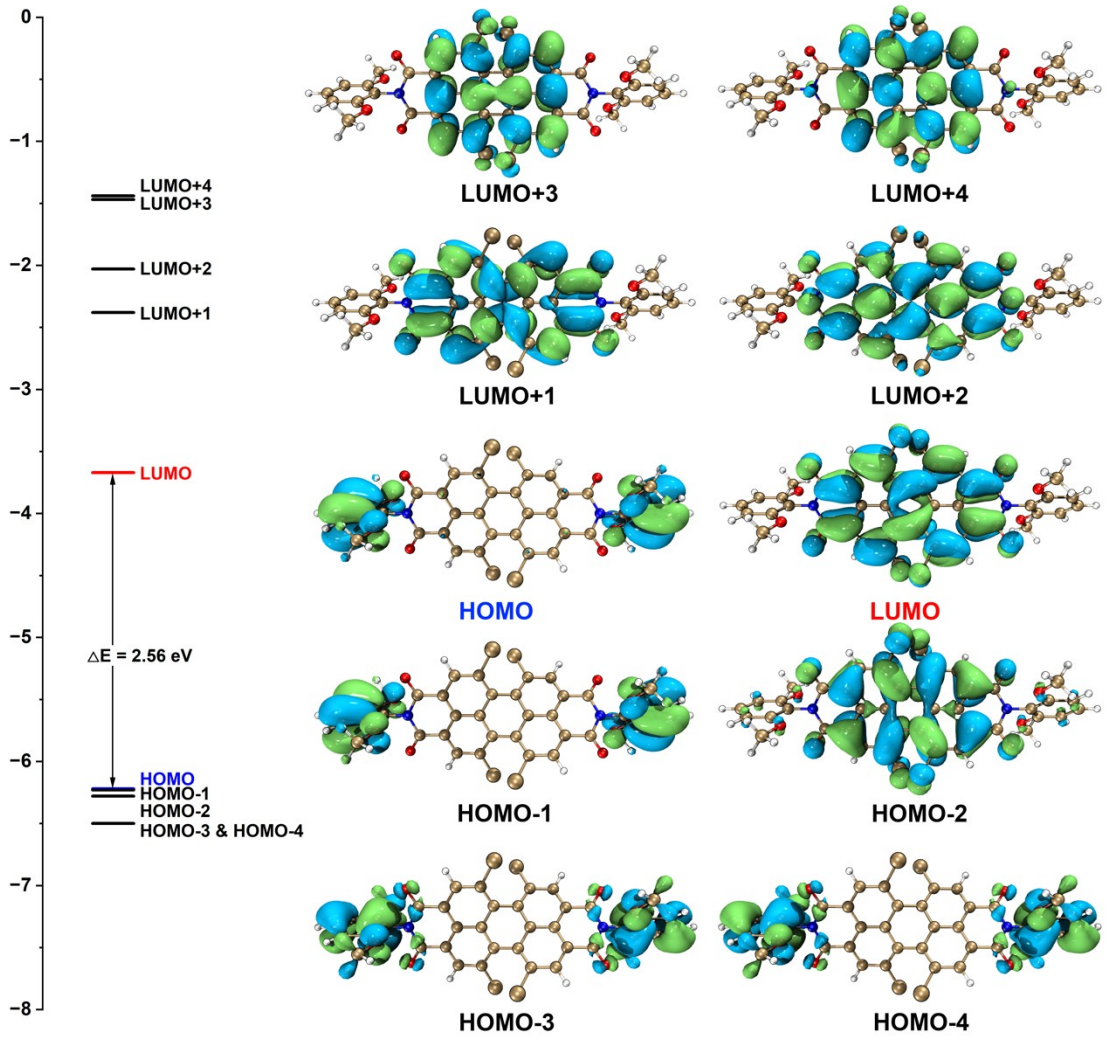

Figure S36. The MO energy diagrams and selected frontier MOs for **PBI-2** calculated at the B3LYP-D3/6-311G(d,p) level.

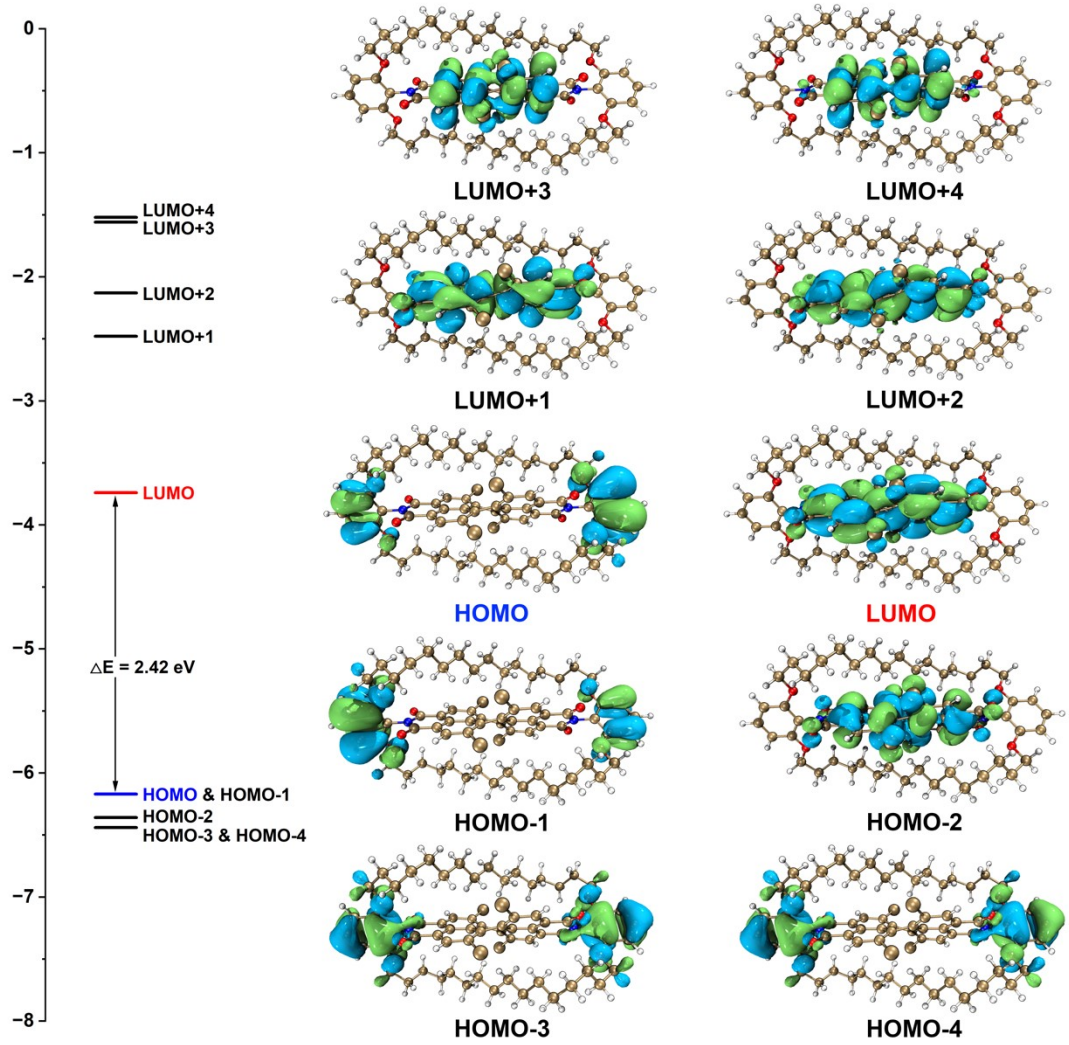

Figure S37. The MO energy diagrams and selected frontier MOs for **Cycle-PBI-4Cl** calculated at the B3LYP-D3/6-311G(d,p) level.

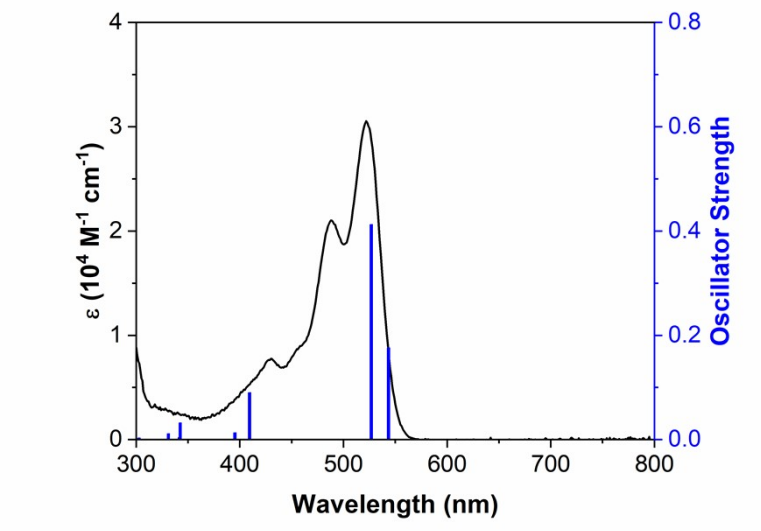

Figure S38. Absorption spectra (solid lines) of **PBI-1** recorded in toluene along with the theoretical vertical transitions (blue bar) obtained from TD-DFT calculations carried out at the B3LYP-D3/6-311G(d,p) level.

Table S8. Selected TD-DFT calculated excitation state energies, oscillator strengths and compositions of the major electronic transitions of **PBI-1** at the B3LYP-D3/6-311G(d,p) level (H = HOMO, L = LUMO).

Excited State	Energy [eV]	Wavelength [nm]	Oscillator Strength (f)	Orbital contributions
1	2.2811	543.53	0.1757	H-2 → L 45.3%, H → L 54.0%
3	2.3529	526.94	0.4127	H-2 → L 53.9%, H → L 45.7%
6	3.0277	409.49	0.0901	H-5 → L 93.8%, H → L+4 4.4%
7	3.1359	395.37	0.0134	H-7 → L 5.4%, H-6 → L 88% H → L+3 3.1%
8	3.1540	393.10	0.0007	H-8 → L+1 4.2%, H-7 → L 87.6% H-6 → L 5.5%
12	3.5436	349.88	0.0006	H-12 → L 10.8%, H-9 → L 4.9% H-2 → L+2 3.8%, H → L+2 78.4%
13	3.5753	346.78	0.0001	H-1 → L+1 98.5%
15	3.6189	342.6	0.0323	H-11 → L 96.7%
16	3.6285	341.69	0.0044	H-14 → L+1 4.5% H-13 → L 91.3%
19	3.7441	331.15	0.0115	H-12 → L 54.4%, H-9 → L 25.6% H → L+2 12.9%, H → L+3 4.4%
23	3.9212	316.19	0.0002	H-2 → L+2 94.1%, H → L+2 4.2%
24	4.0939	302.85	0.0031	H-6 → L 2.0%, H-5 → L+1 64.2% H → L+3 30.2%

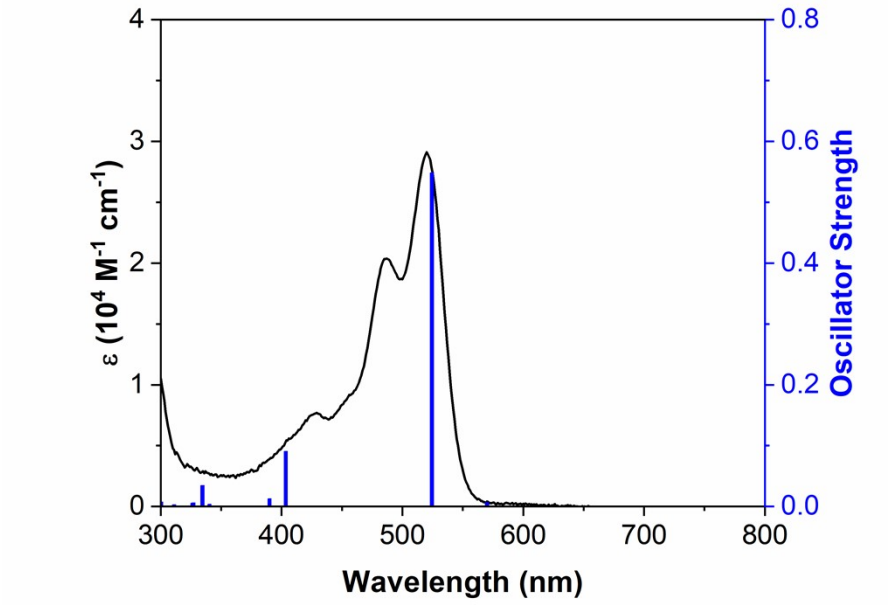

Figure S39. Absorption spectra (solid lines) of **PBI-2** recorded in toluene along with the theoretical vertical transitions (blue bar) obtained from TD-DFT calculations carried out at the B3LYP-D3/6-311G(d,p) level.

Table S9. Selected TD-DFT calculated excitation state energies, oscillator strengths and compositions of the major electronic transitions of **PBI-2** at the B3LYP-D3/6-311G(d,p) level (H = HOMO, L = LUMO).

Excited State	Energy [eV]	Wavelength [nm]	Oscillator Strength (f)	Orbital contributions
1	2.1748	570.1	0.0066	H → L 97.4%
3	2.3637	524.54	0.5486	H-2 → L 97.9%
6	3.0723	403.56	0.0908	H-5 → L 93.2%, H-2 → L+4 5.0%
7	3.1243	396.84	0.0011	H-8 → L+1 4.3%, H-7 → L 85.0% H-6 → L 8.7%
8	3.1313	395.95	0.0004	H-8 → L 93.5%, H-7 → L+1 4.4%
9	3.1779	390.14	0.013	H-7 → L 8.7%, H-6 → L 83.8% H-2 → L+3 3.8%
11	3.4681	357.5	0.0005	H-1 → L+1 98.8%
13	3.4809	356.19	0.0002	H-12 → L 37.3%, H-10 → L 59.0%
14	3.5730	347	0.0011	H-12 → L 4.9%, H-10 → L 9.1% H-2 → L+2 77.9%, H → L+2 5.2%
15	3.6419	340.44	0.0038	H-14 → L+1 4.4%, H-13 → L 91.8%
17	3.6758	337.3	0.0003	H-3 → L+1 95.9%
19	3.7056	334.59	0.0345	H-11 → L 94.7%
21	3.7894	327.18	0.0059	H-12 → L 26.3%, H-10 → L+3 13.9% H-2 → L+3 2.5%, H → L+2 55.3%
23	3.80	326.27	0.0054	H-12 → L 27.4%, H-10 → L+3 11.1% H-2 → L+2 15.3%, H-2 → L+3 3.4% H → L+2 38.0%
24	3.9852	311.11	0.0027	H-3 → L+2 96.9%
26	4.1256	300.53	0.0073	H-6 → L 2.7%, H-7 → L+1 54.4% H-2 → L+3 37.7%, H → L+3 2.3%

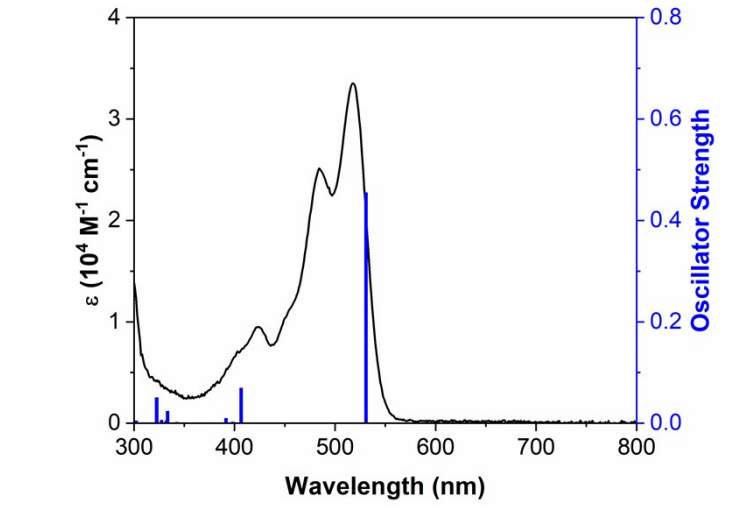

Figure S40. Absorption spectra (solid lines) of **Cycle-PBI-4Cl** recorded in toluene along with the theoretical vertical transitions (blue bar) obtained from TD-DFT calculations carried out at the B3LYP-D3/6-311G(d,p) level.

Table S10. Selected TD-DFT calculated excitation state energies, oscillator strengths and compositions of the major electronic transitions of **Cycle-PBI-4Cl** at the B3LYP-D3/6-311G(d,p) level (H = HOMO, L = LUMO).

Excited State	Energy [eV]	Wavelength [nm]	Oscillator Strength (f)	Orbital contributions
1	2.0388	608.13	0.0002	H → L 98.7%
3	2.2473	551.71	0.0002	H-3 → L 98.3%
4	2.2532	550.26	0.0003	H-4 → L 98.4%
5	2.3350	530.97	0.4548	H-2 → L 99.5%
6	3.0482	406.74	0.0694	H-5 → L 92.7%, H-2 → L+4 4.5%
7	3.1038	399.46	0.0015	H-8 → L+1 0. 5%, H-7 → L 78.4% H-6 → L 15.2%
8	3.1144	398.11	0.0024	H-8 → L 92.1%, H-7 → L+1 4.4%
9	3.1668	391.51	0.0098	H-7 → L 15.0%, H-6 → L 77.0% H-2 → L+3 3.7%
11	3.3086	374.73	0.0001	H-1 → L+1 89.1%, H → L+1 9.7%
13	3.4670	357.62	0.0008	H-12 → L 14.7%, H-10 → L 78.9% H-2 → L+2 3.2%
14	3.5233	351.9	0.0004	H-3 → L+1 97.0%
16	3.5670	347.59	0.0007	H-12 → L 6.5%, H-10 → L 7.0% H-4 → L+1 2.3%, H-2 → L+2 81.0%
17	3.6214	342.36	0.0018	H-16 → L+1 4.6%, H-2 → L 90.8%
18	3.6262	341.91	0.0001	H-16 → L 87.5%, H-15 → L+1 4.6% H-9 → L 2.5%
19	3.6414	340.49	0.0004	H-9 → L 2.1%, H-1 → L+2 76.5% H → L+2 19.1%
20	3.6415	340.48	0.0010	H-1 → L+2 19.4%, H → L+2 79.0%
22	3.7171	333.55	0.0238	H-13 → L 10.0%, H-11 → L 86.3%
24	3.7858	327.50	0.0060	H-12 → L 71.9%, H-10 → L 9.8% H-2 → L+2 8.3%, H-2 → L+3 5.5%
26	3.8428	322.64	0.0504	H-3 → L+2 96.7%
28	4.1025	302.21	0.0048	H-6 → L 2.5%, H-5 → L+1 57.5% H-2 → L+3 37.2%

8. Fluoride Sensing

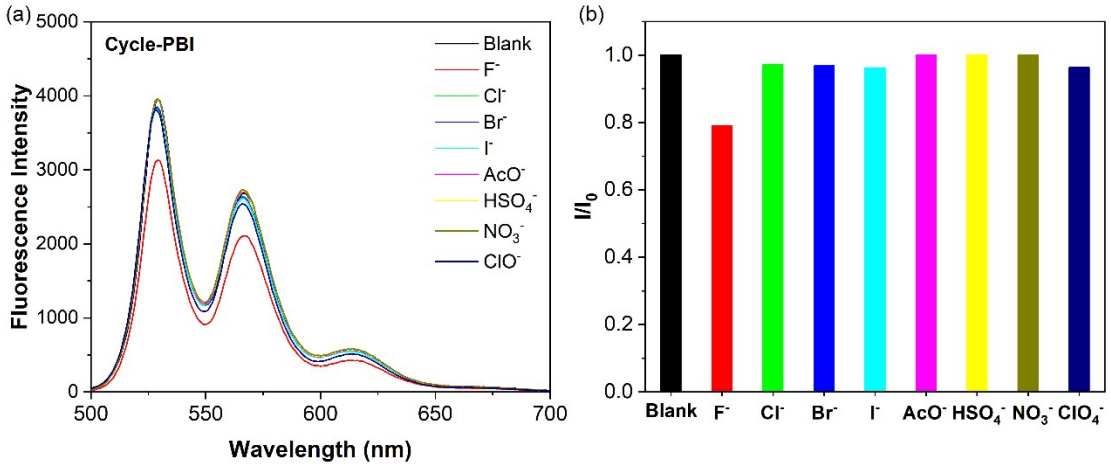

Figure S41. Relative fluorescence intensities of **Cycle-PBI** (10 μM, in THF) upon addition of 2.0 equiv. of various anions (as their tetrabutylammonium salts) including F^-, Cl^-, Br^-, I^-, AcO^-, HSO_4^-, NO_3^-, and ClO_4^-.

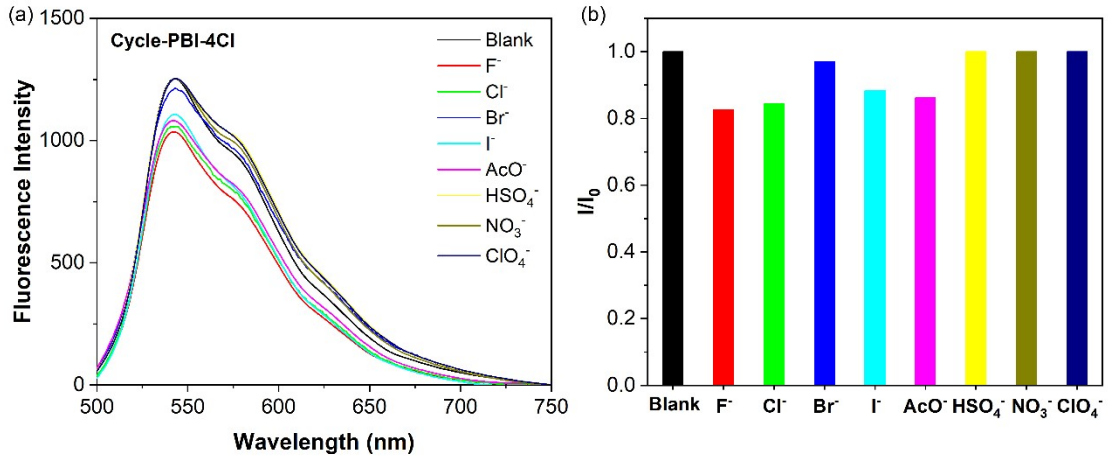

Figure S42. Relative fluorescence intensities of **Cycle-PBI-4Cl** (10 μM, in THF) upon addition of 2.0 equiv. of various anions (as their tetrabutylammonium salts) including F^-, Cl^-, Br^-, I^-, AcO^-, HSO_4^-, NO_3^-, and ClO_4^-.

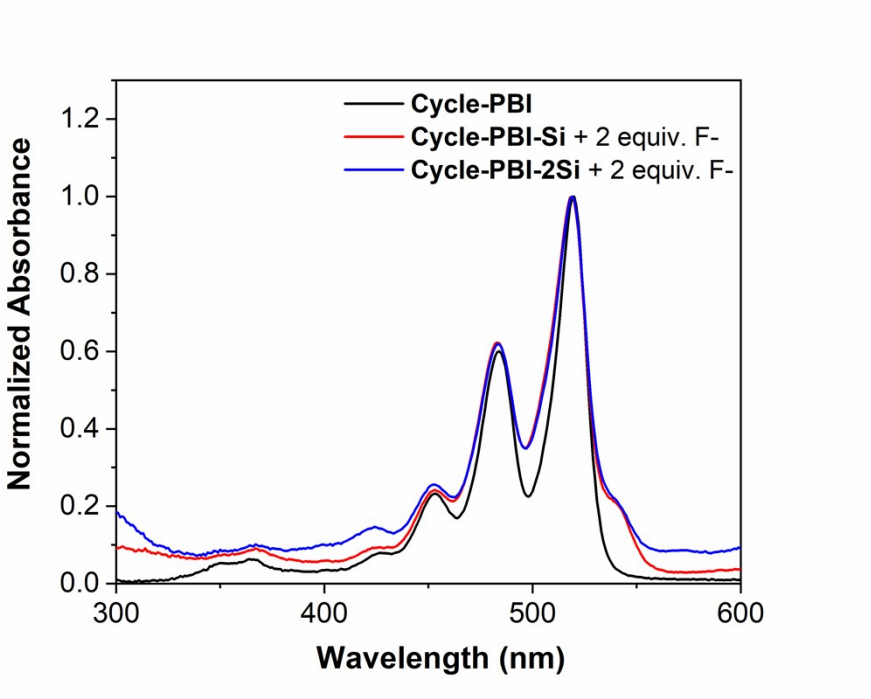

Figure S43. UV-Vis absorption spectra of **Cycle-PBI**, **Cycle-PBI-2Si** and **Cycle-PBI-2Si** after treatment with 2.0 equivalents of fluoride anions in THF solution.

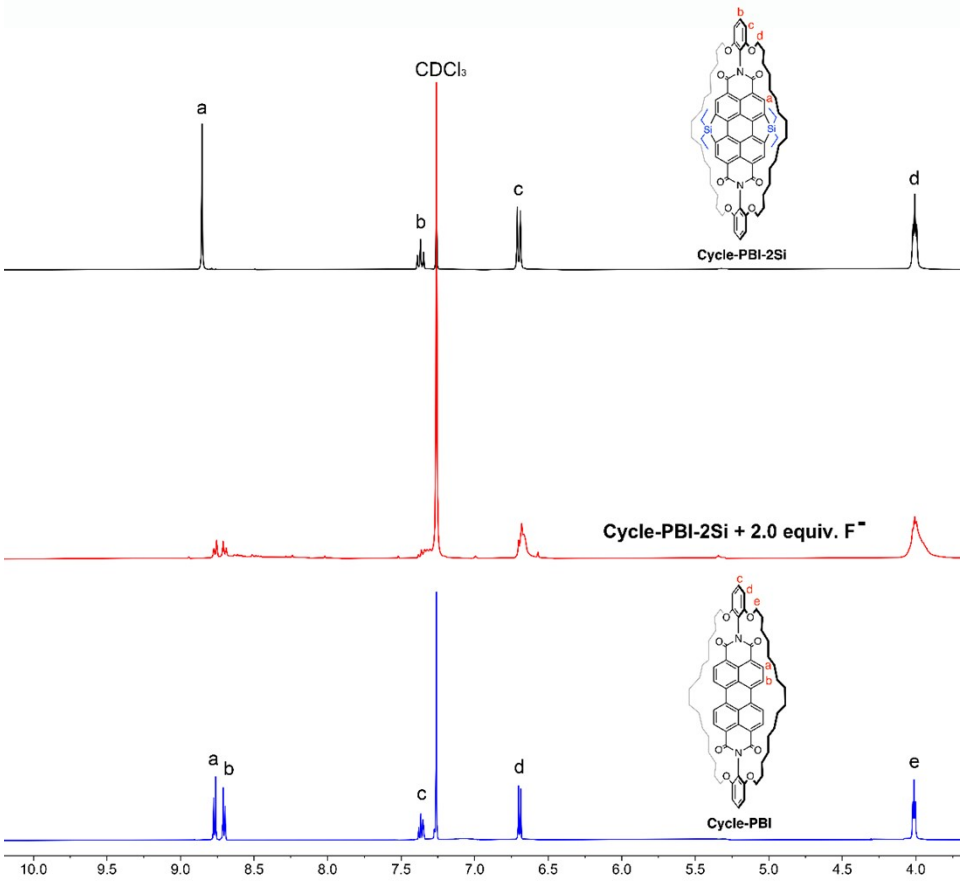

Figure S44. Comparison of partial ^{1}H NMR spectra of **Cycle-PBI**, **Cycle-PBI-2Si** and **Cycle-PBI-2Si** after treatment with 2.0 equivalents of fluoride anions recorded in $CDCl_3$.

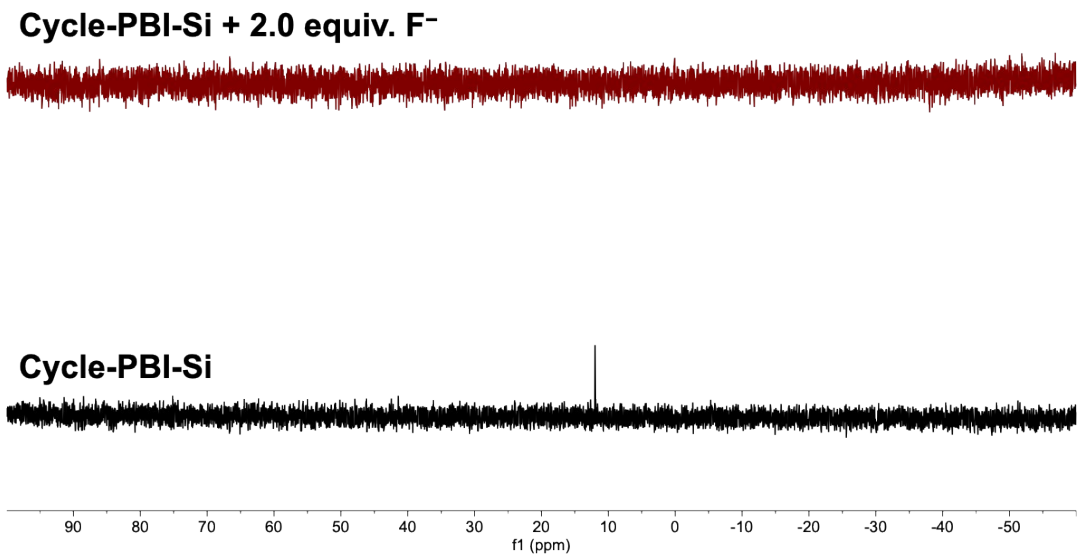

Figure S45. Comparison of ^{29}Si NMR spectra of **Cycle-PBI-Si** before and after treatment with 2.0 equivalents of fluoride anions recorded in $CDCl_3$.

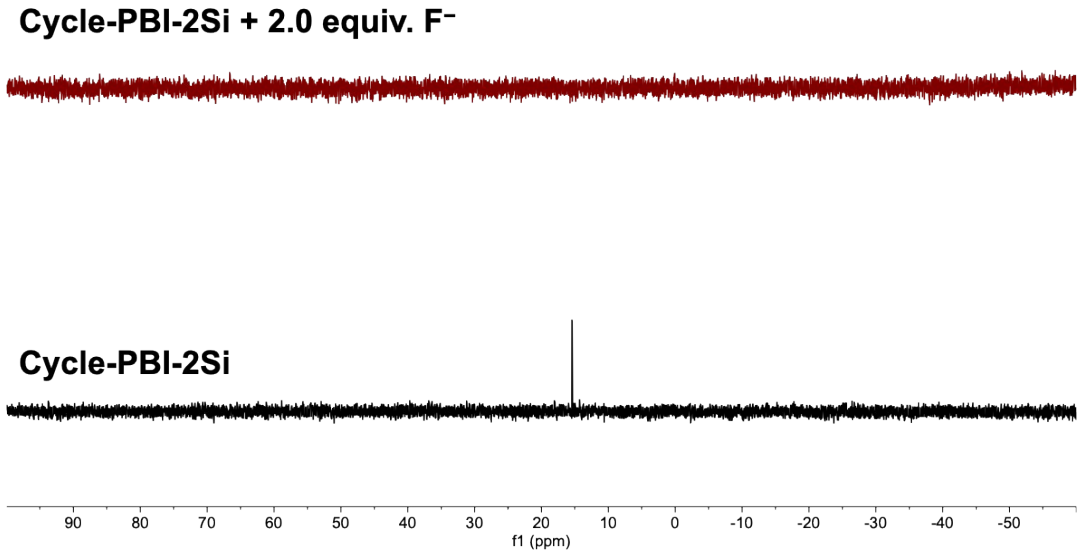

Figure S46. Comparison of ^{29}Si NMR spectra of **Cycle-PBI-2Si** before and after treatment with 2.0 equivalents of fluoride anions recorded in $CDCl_3$.

10. Supporting References

1 L. Zhu, M. Zhang, J. Q. Xu, C. Li, J. Yan, G. Q. Zhou, W. K. Zhong, T. Y. Hao, J. L. Song, X. N. Xue, Z. C. Zhou, R. Zeng, H. M. Zhu, C. C. Chen, R. C. I. MacKenzie, Y. C. Zou, J. Nelson, Y. M. Zhang, Y. M. Sun, F. Liu, *Nat. Mater.,* 2022, **21,** 656-663.

2 M. J. Frisch, G. W. Trucks, H. B. Schlegel, G. E. Scuseria, M. A. Robb, J. R. Cheeseman, G. Scalmani, V. Barone, G. A. Petersson, H. Nakatsuji, X. Li, M. Caricato, A. V. Marenich, J. Bloino, B. G. Janesko, R. Gomperts, B. Mennucci, H. P. Hratchian, J. V. Ortiz, A. F. Izmaylov, J. L. Sonnenberg, Williams, F. Ding, F. Lipparini, F. Egidi, J. Goings, B. Peng, A. Petrone, T. Henderson, D. Ranasinghe, V. G. Zakrzewski, J. Gao, N. Rega, G. Zheng, W. Liang, M. Hada, M. Ehara, K. Toyota, R. Fukuda, J. Hasegawa, M. Ishida, T. Nakajima, Y. Honda, O. Kitao, H. Nakai, T. Vreven, K. Throssell, J. A. Montgomery Jr., J. E. Peralta, F. Ogliaro, M. J. Bearpark, J. J. Heyd, E. N. Brothers, K. N. Kudin, V. N. Staroverov, T. A. Keith, R. Kobayashi, J. Normand, K. Raghavachari, A. P. Rendell, J. C. Burant, S. S. Iyengar, J. Tomasi, M. Cossi, J. M. Millam, M. Klene, C. Adamo, R. Cammi, J. W. Ochterski, R. L. Martin, K. Morokuma, O. Farkas, J. B. Foresman, D. J. Fox, Gaussian 16, Revision A03; Gaussian, Inc.: Wallingford, CT, 2016.

3 T. Lu and F. Chen, *J. Comput., Chem.,* 2012, **33**, 580-592.

4 T. Lu, *J. Chem. Phys.,* 2024, **161**, 082503.